NAME [redacted]

DATE 05/13/2013

UNIVERSITY OF OKLAHOMA

GRADUATE COLLEGE

NUMERICAL SIMULATION OF TRANSIENT CUTTINGS TRANSPORT WITH FOAM IN HORIZONTAL WELLS

A THESIS

SUBMITTED TO THE GRADUATE FACULTY

in partial fulfillment of the requirements for the

Degree of

MASTER OF SCIENCE

By

SAMIR PRASUN
Norman, Oklahoma
2013

NUMERICAL SIMULATION OF TRANSIENT CUTTINGS TRANSPORT WITH FOAM IN HORIZONTAL WELLS

A THESIS APPROVED FOR THE
MEWBOURNE SCHOOL OF PETROLEUM AND GEOLOGICAL ENGINEERING

BY

[redacted]

Dr. Ramadan Ahmed, Chair

[redacted]

Dr. Subhash Shah

[redacted]

Dr. Faruk Civan

ACKNOWLEDGEMENTS

I would like to express my deepest gratitude to my advisor, Dr. Ramadan Ahmed, for his guidance, encouragement and constant support throughout my study.

I would also like to thank Dr. Subhash Shah and Dr. Faruk Civan for their participation in my thesis committee, and taking time out of their busy schedule to review my work. Moreover, their courses have served me helpful for conducting this research.

I am also thankful to other professors and colleagues of the Mewbourne School of Petroleum and Geological Engineering for their help during my graduate study.

Finally, I would like to thank my parents for their unconditional support and love during my whole graduation tenure at The University of Oklahoma.

TABLE OF CONTENTS

LIST OF TABLES

LIST OF FIGURES

ABSTRACT

The use of foam for underbalanced drilling applications is increasing significantly. This is because foam exhibits properties, which are desirable when drilling depleted and low-pressure wells. However, a good knowledge of foam hydraulics and cuttings transport (hole cleaning) is essential for successful applications of foam drilling technology. Cuttings transport with foam in inclined wells is still less understood. Change in inclination makes it difficult to predict the bed height and pressure profiles along the wellbore. Variations in drilling parameters have significant effects on the foam properties and cuttings transport mechanisms. This investigation focuses on understanding the effects of drilling parameters on the cuttings concentration and pressure profiles. Properly designed foam drilling requires efficient hole-cleaning thus avoiding any lost circulation, formation damage and stuck-pipe.

A new transient wellbore hydraulics and cuttings transport model has been developed. The model incorporates frictional pressure loss and hydrostatic pressure change occurring in the wellbore, and it predicts foam flow properties (density, viscosity, velocity, quality, and pressure) at different depths of the wellbore.

In order to predict the cuttings bed formation in horizontal wells, a mechanistic hole-cleaning model consisting of two layers has been utilized. The model is based on torque balance for a particle on the surface of a bed formed in build-up or horizontal section of a wellbore. In addition, a new model has been formulated for the local shear stress and local fluid velocity in the eccentric annulus to be applied in the torque and force balance equations. A computer program (simulator) has been developed to solve

the model equations using finite difference method to calculate cuttings concentration and pressure profiles as a function of time.

Model predictions were compared with published experimental data and the model is fine-tuned to minimize discrepancies. Extensive parametric study was conducted to investigate the effects of different drilling parameters on cuttings concentration and pressure profiles. Results show how the cuttings bed front moves up in the annulus along the build-up and horizontal sections. A detailed sensitivity analysis of the effects of gas and liquid flow rates, foam quality, and back pressure on the cuttings concentration and pressure profiles was performed. The effect of inclination on the equilibrium bed height and critical foam velocity were studied in detail. The model also takes into account the liquid influx during underbalanced drilling. Parametric study on the effects of liquid influx on the foam properties and cuttings concentration was conducted.

Model predictions showed a good match with experimental results for concentric horizontal annulus except at higher polymer concentrations (greater than 0.25%). The simulation results show that bed height and bottom-hole pressure are quite sensitive to the changes in surface foam injection rates and back-pressure, thereby can be best optimized by properly adjusting the input parameters. In extreme underbalanced conditions, water-influx can result in reduction of foam quality (as much as 23%) without affecting much of its hole-cleaning performance. The result also suggests that hole-cleaning is a function of inclination. The bed height increases with increase in inclination angle until a critical angle of 90^{o}-φ (φ is the angle of repose) after which, it reduces.

CHAPTER 1: INTRODUCTION

Foam is a dispersion of gas in liquid-phase stabilized by surfactant molecules. The liquid is a continuous phase. Gas is dispersed as bubbles separated by liquid films known as lamellae. Foam quality is the most important property of foam that affects it properties. Foam quality represents the volume fraction of gas-phase in the foam. Hence:

$$\Gamma = \frac{V_g}{V_g + V_L} \tag{1.1}$$

where, V_g is the volume of the gas phase and V_L is the volume of liquid phase. At high qualities (greater than 97.5%), foam becomes unstable and turns into mist. The liquid-phase disperses in the gas-phase which becomes continuous. Foam is characterized as dry or wet foam depending on its quality (Fig. 1.1). When the quality ranges between 95% - 97.5%, it is classified as dry foam, and its bubbles tend to form polyhedral structure separated by thin film of liquid and have thin lamellae. On the other hand, at a medium quality range (55%-95%), it is classified as wet foam, and the bubbles are more likely to have a spherical or polyhedral shape and have thick lamellae.

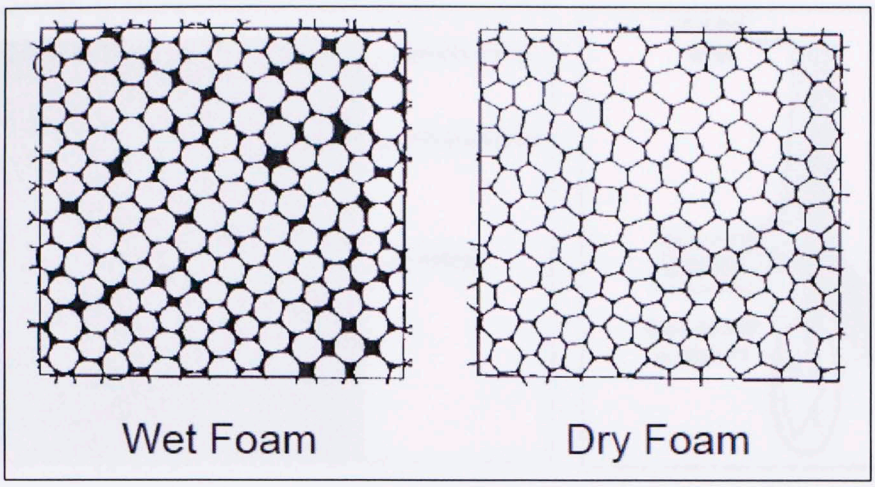

Fig. 1.1 Structure of wet foam vs. dry foam

Foams used in drilling operations are generated by mixing gas phase and liquid phase that contains surfactant at low concentration (<3%). Often it is created either by the shearing action of gas injection (nitrogen or carbon dioxide) into the liquid or vigorous agitation of the two phases in the presence of surfactant. Aqueous foams utilize water as a base liquid phase. A foam bubble can be described as consisting of lamellae, plateau borders and nodes/vertexes (Ibizugbe 2012). The lamellae are the liquid films that separate the adjoining bubbles. Usually when three or four bubbles of high quality foam meet, the bubbles form of polyhedral structure. At the junction, liquid films are curved and meet at a line forming what are called plateau borders. The nodes are the junctions of plateau borders (Fig. 1.2). Typically, in wet foams, bubbles are monodisperse in shape while they become polydispersed at higher quality dry foams.

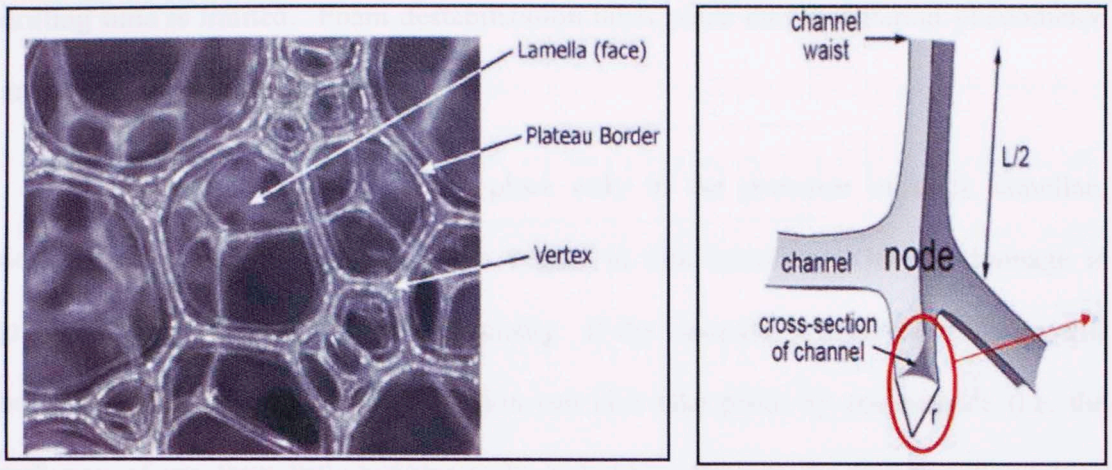

a) b)

Fig.1.2 a) Foam structure (Von Phul and Stern 2004); and b) node (Koehler et al. 1999)

The stability of foam is improved by addition of surfactant and polymers. A molecule of surfactant possesses surface activity. It consists of a polar hydrophilic (water-soluble) head group and a non-polar hydrophobic (oil soluble) tail group. Surfactant molecules associate with each other at high concentrations, thereby forming micelles. Micelles are clusters of surfactant molecules having hydrophobic hydrocarbon tails preferentially adsorbed with the gaseous phase while the hydrophilic heads remain preferentially attached with the liquid phase. This reduces the surface tension at the foam interface which reduces diffusion of gas through the liquid films and thus creating a foam system that have a longer life.

Foam is a thermodynamically unstable fluid system. When its quality falls below 55%, it tends to segregate itself into individual components quickly to release the free energy. For stiff foams containing stabilizing polymers, the segregation phenomena which leads to instability is a time-taking process; hence its adverse effect during the

drilling time is limited. Foam destabilization takes place due to different phenomena: gravity drainage and coalescence.

While gravity drainage takes place only in the presence of thick lamellae, destabilization due to surface tension begins in thin lamellae. Gravity drainage is greatly influenced by liquid-phase viscosity. If the viscosity is high, the drainage will be slow and vice-versa. Destabilization can also take place by coalescence (i.e. the diffusion of gas from little bubbles to large bubbles through the thin lamellae which occurs in the direction of decreasing pressure). Understanding foam stability after sand addition becomes more complex due to the resulting changes in bubbles surface properties and viscosity of the liquid phase.

Since foam is a light weight fluid, it is widely being used in underbalanced drilling. Advantages of underbalanced drilling are numerous as it prevents formation damage, lost circulation, clay swelling and stuck pipe. Less formation damage helps in good formation evaluation preventing any error detection caused by the mud filtration losses. Underbalanced drilling helps maintaining the efficiency of the bit resulting in higher ROP and increased bit-life. This saves considerable time and resource during drilling operation. Also, higher viscosity of foam leads to higher cuttings carrying capacity and hence, facilitates hole-cleaning. However, there are also reasons, which make foam difficult to use in underbalanced drilling. Difficulties in predicting foam stability is one primary reason. And foam being non-Newtonian and structured fluid, it becomes difficult to predict its rheological properties, which vary substantially with pressure and temperature. Foam properties including quality, density, viscosity, velocity, vary significantly with depth due to its compressible nature. Prediction of

these properties becomes more difficult in extreme underbalanced conditions when the liquid influx further degrades the stability of foam and obscures the foam flow behavior. Furthermore, foam drilling requires an expensive set-up for the foam generation and surfactant agitation and hence, necessitates the great deal of skills and experience in this field.

CHAPTER 2: PROBLEM STATEMENTS AND GOALS

Today, many of the existing oil reservoirs have pore pressures below the hydrostatic pressures exerted by the lightest drilling fluids during conventional drilling. As a result, underbalanced drilling has become the preferred technique in drilling depleted reservoirs. However, successful application of underbalanced (foam) drilling still remains to be the major concern in directional wells. This chapter deals with the description of the problem, urgent need for this research and the value this work is set to achieve in the petroleum industry.

2.1 Statement of Problem

Foam is widely preferred as a fluid in underbalanced drilling because of its light weight and high viscosity. However, there are some problems which makes foam a difficult fluid to use during underbalanced drilling. Foam complexities pose a significant problem in predicting rheological and hydraulic parameters of foam in high-pressured down-hole conditions. Though correlations have been developed to predict aqueous foam rheology as a function of quality, these correlations do not provide accurate predictions when polymers or viscosifiers are added. Moreover, these correlations do not account for degradation occurring in foam with time under downhole condition. Hence, they may lead to misrepresentation of rheology.

In inclined and horizontal wells, prediction of the flow parameters such as bottom hole pressure (BHP), foam velocity, density and viscosity becomes a challenging task.

Major difficulty in application of foam drilling in directional well is to keep the bed height under control (hole-cleaning) and maintain the bottom-hole pressure below the pore-pressure at the same time. Hence, proper understanding of foam properties and cuttings transport during foam drilling becomes necessary. Inaccurate prediction of foam properties and uncertainty in reservoir pressure can lead to undesirable downhole conditions. It may cause extreme underbalance resulting in liquid influx or overbalance resulting in significant loss of foam fluid. Hence, knowledge of liquid or gas influx and its dynamic impact on the foam properties during foam drilling becomes necessary.

Due to increase in drilling of horizontal and inclined wells, focus is being shifted from foam drilling in vertical wells to inclined and horizontal wells. Cuttings transport models have already been developed for vertical and inclined wells based on force and torque analysis on a single cuttings particle under steady state conditions. The major challenge is to develop a transient cuttings transport model that can make prediction of cuttings concentration and pressure profile before steady state condition is established in the wellbore.

Calculation of local stress and velocity in the eccentric annulus is required in torque balance equations to correctly estimate the bed height in inclined and horizontal wells. This will also ensure the accurate prediction of bottom-hole pressure. Though the estimation of local fluid velocity is simple in case of concentric annulus, the difficulties arise in partially blocked eccentric annulus due to non-uniform and relatively complex annular velocity profile. Hence, due to the above challenges, this research project is a unique study on understanding the problems of the foam drilling in the three segment wells and bringing a practical solution to mitigate these problems.

2.2 Objectives

Following are the objectives for conducting the study on the cuttings transport in foam:

i. Predict the foam hydraulics parameters including quality, density, viscosity, velocity and pressure along the wellbore.

ii. Understand the behavior of cuttings-bed formation during foam drilling.

iii. Investigate the effects of drilling parameters on the foam properties, cuttings concentration and pressure profiles along the wellbore.

iv. Study the effects of hole inclination on bed height and local critical velocity along the build-up and horizontal sections.

v. Predict the water-influx while drilling underbalanced in a water-sensitive zone and study its impact on foam properties and hole-cleaning.

2.3 Approach

In order to achieve the goals, the following procedures were followed during the study:

i. Extensive literature review and theoretical study was performed to understand and model foam hydraulics and foam-cuttings transport in inclined and horizontal wells.

ii. Using Chen's (2005) rheological correlations and momentum conservation equations, a computer code (simulator) was developed to predict foam properties along the well bore. Local fluid velocity is required in the momentum equations to predict the equilibrium bed height. Hence, a new model has been

formulated to estimate the local stress and fluid velocity near cutting bed surface in eccentric annulus.

iii. In the vertical section, forces acting on a cuttings particle were analyzed to derive slip velocity equation; and in build-up and horizontal sections, moments acting on a flow-protruding bed particle were considered to predict equilibrium bed height.

iv. Model predictions were verified with the published experimental data and the model is fine-tuned to minimize discrepancies.

v. Equations of continuity and conservation of momentum were used to build a transient model for predicting cuttings concentration and pressure profiles as a function of time during foam drilling.

vi. Sensitivity analysis was performed to investigate the effects of drilling parameters on the cuttings transport during foam drilling. Study was also conducted to examine the effects of inclination on cuttings concentration and pressure profiles.

vii. Drawdown equations were utilized to predict the water-influx in underbalanced condition in water-sensitive zone and investigate its effect on the foam hydraulics, cuttings concentration and pressure profiles.

CHAPTER 3: LITERATURE REVIEW

Foam rheology and hydraulics have widely been studied in the past for various applications of drilling and completions. Cuttings transport in foam is still less understood especially when the well deviates from vertical to horizontal. Both experimental and mathematical approaches have been developed in the past to study foam hydraulics and its effect on cuttings transport. In this review, special emphasis is given on experimental studies and model of: i) foam rheology; ii) foam hydraulics; and iii) cuttings transport with foam.

3.1 Foam Rheology

Foam quality and liquid base viscosity are the dominant factors affecting the rheology of foam. For wet foams, Hatschek (1911) mathematically developed a rheological model that is dependent on the foam quality and liquid base viscosity. The model is given by:

$$\mu_F = \frac{\mu_L}{1-\Gamma^{.33}} \tag{3.1}$$

Based on the experimental results, Mitchell (1969) modified the correlation by changing the exponential constant from 0.33 to 0.49. Hence:

$$\mu_F = \frac{\mu_L}{1-\Gamma^{.49}} \tag{3.2}$$

From Fig. 3.1, it can be noted that as foam quality increases, foam apparent viscosity exhibits a different trend with respect to quality. There are four different

regions which can be classified based on the range of foam quality; i) dispersed bubble region ($0 \leq \Gamma \leq 55\%$) ; ii) wet foam region ($55\% \leq \Gamma \leq 95\%$) ; iii) dry foam region ($95\% \leq \Gamma \leq 97.5\%$); and iv) mist region ($97.5\% \leq \Gamma \leq 100\%$).

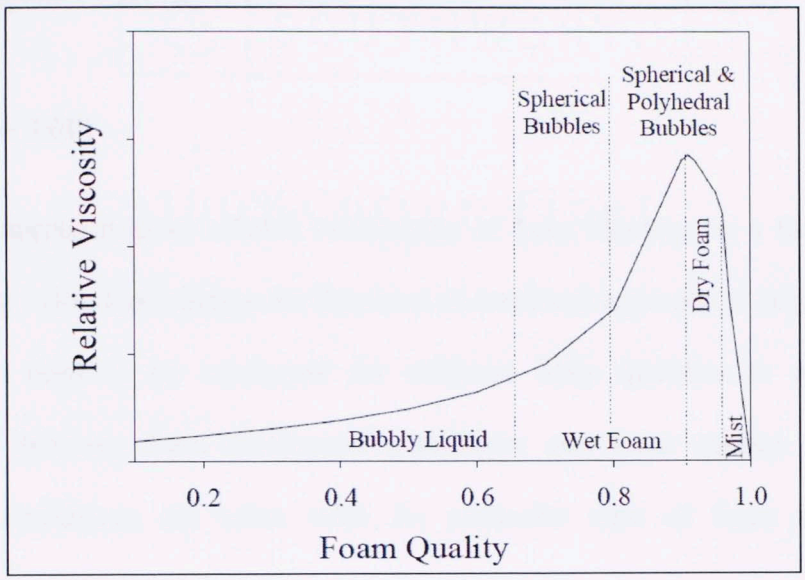

Fig. 3.1 Foam viscosity vs. quality (Ahmed et al. 2003a)

As the quality is increased beyond the bubbly liquid region, foam becomes rigid and spherical in shape. Further increase changes the foam structure from spherical to polyhedral configuration. Consequently, bubble deform against their neighbors. Increasing the quality of foam beyond the wet region degrades the viscosity of foam until it reaches the foam stability (inversion) point. Beyond the foam stability point, the viscosity decreases rapidly to reach the gas viscosity. The stability limit of water-based foam is 97.5%.

Literature survey shows that foam rheology can be modeled applying different approaches: i) empirical; ii) semi-empirical; and iii) mathematical. The relationship

between foam viscosity and foam quality can be determined by conducting experiments. The rheology model which best fit the experimental data is chosen as the rheological correlation of that particular foam. In the bubbly liquid region, Mitchell (1969) found that foam apparent viscosity is related to its quality and liquid viscosity by:

$$\mu_F = \mu_L(1 + 3.6\Gamma) \tag{3.3}$$

This approach gives reliable relationship of foam rheology as a function of its quality. The main disadvantage for this kind of empirical approach is large number of experiments need to be conducted for different foam qualities to establish the relationship between foam rheological parameters and foam quality. Moreover, empirical correlations are often valid for particular type of foam used in the experiments.

Based on experimental results obtained from pipe viscometer, Shah and Khade (2004) developed rheological models (correlations) for guar foams. The models predict power law fluid parameters (K and n) and, thus, the apparent viscosity of foam. They carried out extensive foam rheology experiments with aqueous and gelled water foams using N_2 as gas phase at pressure of 1,000 psia and temperature ranging between 100 to 200°F. Guar gel was used as a base liquid phase. They concluded that both fluid consistency index and fluid behavior index of guar foam are functions of quality and their respective liquid-phase consistency index and flow behavior index. For 20 lbm/Mgal guar foam, the following correlations are given:

$$\frac{n_{Foam}}{n_{Liquid}} = 1 - 2.1006\Gamma^{7.3003} \tag{3.4}$$

$$\frac{k_{Foam}}{k_{Liquid}} = e^{(-1.9913\Gamma + 8.9722\Gamma^2)} \tag{3.5}$$

where, n_{Foam} is the foam behavior index and n_{liquid} is the base liquid behavior index.

The semi-empirical approach uses the application of chemical engineering. According to this approach, foam viscosity is a function of bubbles size, interfacial tension, liquid viscosity and the stability of foam. Another semi-empirical approach for foam rheology modeling is based on volume equalized principle given by Valko and Economides (1992). It states that any rheological model can be transformed to volume-equalized form. Power law model used for characterizing foam fluid can be converted to volume-equalized form by:

$$\frac{\tau}{\epsilon} = K_{vE}\left(\frac{\gamma}{\epsilon}\right)^n \tag{3.6}$$

where, ϵ is the specific volume expansion ratio, given by $\epsilon = \frac{\rho_{liquid}}{\rho_{foam}}$, and K_{vE} and n are the rheological parameters for a given mass flow rate at a given temperature. It means that the volume equalized rheological model for particular foam is independent of the foam quality. There is one unique curve characterized by volume-equalized shear stress and volume-equalized shear strain for a given mass flow rate valid for all foam qualities. Since the approach has been designed primarily for the fracturing foam fluid where the foam quality is around 70%, it can give erroneous results if applied to drilling foams where foam quality can go as high as 95%.

3.2 Foam Hydraulics

A number of foam hydraulics models (Blauer et al. 1974; Sanghani 1982; Valko and Economides 1992; Gardiner et al. 1998; Lourenco 2002; Ahmed et al. 2003b; Chen 2005) were developed in the past to predict the pressure loss. These models were developed assuming laminar flow conditions because foam flow during drilling predominantly lies in the laminar regime.

Foam is a compressible non-Newtonian fluid; its properties including foam density, viscosity and velocity vary with depth. Foam apparent viscosity can be estimated using empirical models with foam quality and shear rate. The rheology model along with the equation of state can be used in predicting hydraulic properties of foam.

In the development of hydraulic model for foam, Blauer et al. (1974) assumed the foam to be Bingham plastic fluid and derived the frictional pressure loss formulas for laminar, transitional and turbulent flows. Foam plastic viscosity and yield strength were determined as a function of foam quality. In the model, foam density is estimated by ignoring the weight of gas phase. For turbulent flow, pressure loss is calculated using Moody diagram. For laminar pipe flow, pressure loss is determined using the Buckingham-Reiner equation:

$$Q = \frac{\pi D^3 \tau_w g_c}{32 \mu_p} \left(1 - \frac{4}{3}\frac{\tau_y}{\tau_w} + \frac{1}{3}\left(\frac{\tau_y}{\tau_w}\right)^4 \right) \tag{3.7}$$

Applying the momentum balance, the wall shear stress (τ_w) in Eq. (3.5) can be written as a function of pressure loss and pipe geometry:

$$\tau_w = \frac{\Delta P}{L}\frac{D}{4} \tag{3.8}$$

A foam hydraulic model, similar to that of Blauer et al. (1974), was presented by Sanghani (1982). The main difference between these two models is that Sanghani model assumes the foam to be a Pseudo-plastic fluid. The rheological parameters for Pseudo-plastic model, 'K' and 'n' are determined as a function of foam quality. In addition, foam density calculation takes into account gas phase density change. However, Blauer et al. ignored the weight of the gas in foam density predictions. The pressure drop for laminar flow of foam in pipes was determined using the following hydraulic model developed for incompressible fluids:

$$\frac{\Delta P_f}{\Delta L} = \frac{4K}{D}\left(\frac{8(3n+1)Q}{\pi n D^3}\right)^n \tag{3.9}$$

Wall slip is one of the phenomena that complicate foam hydraulic modeling. Beyer et al. (1972) considered the effect of wall slip in their hydraulic modeling of foam flow. They described the composition of foam in terms of liquid volume fraction, which is defined as:

$$LVF(T,P) = 1 - \Gamma \tag{3.10}$$

Total foam velocity (v_T) is composed of slip component (v_s) and a fluidity component (v_F), which can be expressed as:

$$v_T = v_s + v_F \tag{3.11}$$

They introduced an explicit function, Ψ which is used to determine the frictional pressure drop as a function of total velocity (v_T), liquid volume fraction (LVF) and pipe diameter (D) as follows:

$$\left(\frac{dP}{dL}\right)_f = \frac{4\Gamma_w}{D} = \Psi[v_T, \Gamma, D] \tag{3.12}$$

For compressible fluids like foam, v_T and Γ are functions of pressure and temperature.

Foam velocity changes as it flows in the wellbore due to expansion resulting from pressure change. As a result, flow parameters such as foam density and Reynolds number vary in the wellbore. Valko and Economides (1992) proposed volume-equalized Reynolds number to calculate the friction factor in the wellbore. This prevented any dependence on the foam quality on the flow characterization. By using the 'specific volume expansion ratio', the normalization of any density dependent parameters was possible. For power-law fluids, the volume-equalized Reynolds number and volume-equalized fanning friction factor were given by:

$$N_{ReVE} = \frac{D^n u^{2-n} \rho}{K \epsilon^{1-n}} \tag{3.13}$$

$$f_f = \frac{2}{N_{ReVE}} \left(\frac{6n+2}{n}\right)^n \tag{3.14}$$

Applying the mechanical energy balance, following equation was developed for calculating frictional pressure losses in horizontal pipes:

$$\frac{dp}{dx} = -\frac{1}{D} \frac{(2f_f b^2 c^2 - Dg)p^3 + 4f_f abc^2 p^2 + 2f_f a^2 c^2 p}{bp^3 + ap^2 - abc^2 p - a^2 c^2} \tag{3.15}$$

where, the constants a, b and c are defined as follows:

$$a = w_g \frac{RT}{M_g}, b = w_g \frac{RTB}{M_g} + (1 - w_g)\frac{1}{\rho_g}, c = \frac{4(m_g + m_L)}{\pi D^2}, w_g = \frac{m_g}{m_g + m_L} \tag{3.16}$$

Gardiner et al. (1998) was the first to utilize the volume-equalized principle proposed by Valko and Economides (1992) and account for the wall-slip in friction pressure loss calculation. They considered volume-equalized Pseudo-plastic rheology model to describe flow behavior of foam.

$$\tau = k\epsilon^{1-n}(\frac{du}{dr})^{n-1}\frac{du}{dr} \tag{3.17}$$

An equation analogous to Hagen-Poiseuille pipe flow formula was derived for volume-equalized power law fluid:

$$Q_{calculated} = 2\pi \int_0^R urdr = \pi R^2 \left\{u_{slip} + \frac{n}{3n+1}\left[-\left(\frac{dp}{dx}\right)\frac{R^{n+1}\epsilon^{n-1}}{2k}\right]^{\frac{1}{n}}\right\} \tag{3.18}$$

The volume-equalized approach was also used by Lourenco (2002) to study foam flow in pipe and annulus under high pressure high temperature conditions. He utilized the volume-equalized power law rheological model and developed the hydraulic model similar to that of Gardiner (1998). The main difference is that Lourenco (2002) used the effective diameter for foam flow in annulus.

Another approach for foam hydraulic modeling is to consider varying foam properties in the wellbore. Such approach requires a numerical procedure to determine foam properties (quality, density, velocity and viscosity) at different depths of the wellbore. Ahmed et al. (2003b) developed a numerical model for foam flow in annulus during drilling operation. The model predicted foam properties and hydraulic parameters including density, quality, viscosity, velocity and pressure as a function of

depth for various operating variables. The model is based on mechanical energy balance:

$$\frac{dP}{\rho} + udu = -\left(\frac{2fu^2}{D} + gcos\theta\right) dL \tag{3.19}$$

In order to obtain numerical solutions, pipe and annulus were divided into computational segments and the above equation was applied in discrete form for each segment to estimate foam properties and hydraulic parameters of the flow. More recently, a similar numerical model (Chen 2005) has been developed using the conservation of momentum. Chen (2005) used the following equation to indirectly calculate foam density at different depths.

$$\rho_F = \frac{P}{a+bP} \tag{3.20}$$

where,

$$a = \frac{RTW_g}{M} \quad \text{and} \quad b = \frac{BW_g}{M} + \frac{1-W_g}{\rho_L}$$

In the above equation, b is the 2nd viral coefficient of gas.

Mass fraction of gas, W_g, is given by:

$$W_g = \frac{m_g}{m_L+m_g} \tag{3.21}$$

Dividing the wellbore into segments and integrating the momentum equation between two adjacent nodes of segments, following equation can be obtained:

$$\Delta L = \frac{\left[(P_1-P_2)+\beta\frac{m}{A}(V_1-V_2)\right]D_h}{4\tau_w+\rho g D_h cos\alpha} \tag{3.22}$$

where, P_1 *and* P_2 are the pressures at adjacent nodes, ΔL is the distance between the nodes, ρ is the average foam densities in the segment, τ_w is the average wall shear stress between Node 1 and Node 2, as shown in the schematic presented in Fig. 3.2. Chen (2005) applied the above model to determine foam properties in a three-segment well (vertical section, inclined section and horizontal section). Input parameters used in the foam hydraulic simulation are listed in Table 3.1. Description of the three-segment well is presented in Table 3.2.

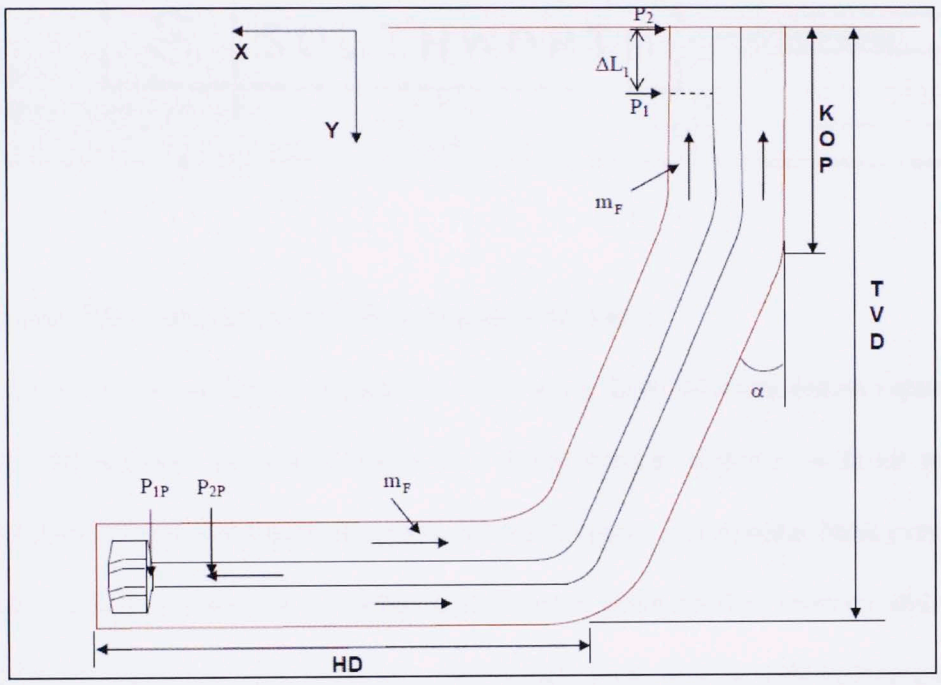

Fig. 3.2 Schematic of foam flow in three-segment wellbore (Chen et al. 2005)

Table 3.1 Input data for foam hydraulic simulation (Chen 2005)

Parameters	Value
Liquid density (lbm/ft^3)	62.4
Liquid flow rate (gpm)	40
Gas flow rate (scf/min)	1200
Temperature gradient (°F/100 ft)	1.5
Surface temperature (°F)	80
Surface back pressure (psia)	100
Hole size (inch)	8.5
Drill pipe OD (inch)	5

Table 3.2 Three-segment wellbore description (Chen 2005)

	Section Length (ft)	Inclination (degrees)
Section 1: Vertical section	3000	0
Section 2: Inclined section	3000	45
Section 3: Horizontal section	4000	90

3.2.1 Foam Flow Simulation in Three-Segment Wellbore

Chen (2005) conducted simulation study using three different foams representing aqueous and polymer thickened foams in a three-segment wellbore with air injection rate of 1200 scf/min and liquid injection rate of 40 gpm, and annular back pressure of 100 psia. Figures 3.4 through 3.7 depict the pressure, foam quality, velocity and density profiles in the three-segment wellbore. The results show that as well inclination angle increases the changes in foam and flow properties (pressure, foam quality, foam density and foam velocity) with respect to measured depth decrease. This is because of reduction in the axial component of the weight of the foam. When the well profile changes from inclined to horizontal, there is no axial component of the weight and hence the main change in pressure gradient is due to friction loss. Hence, he concluded

that foam properties in horizontal and highly inclined sections of a wellbore remain intact and approximately uniform.

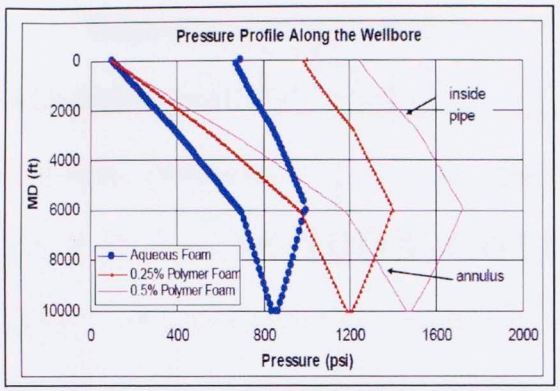

Fig. 3.3 Pressure vs. depth in three-segment well (After Chen 2005)

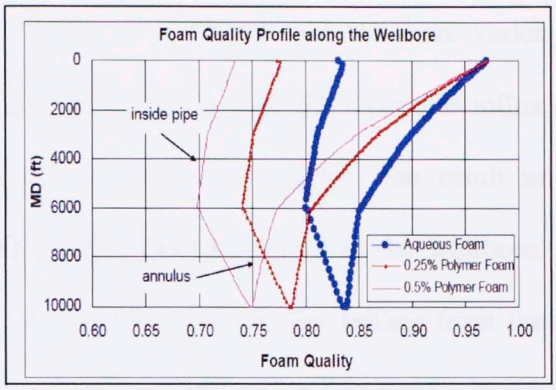

Fig. 3.4 Foam quality vs. depth in three-segment well (After Chen 2005)

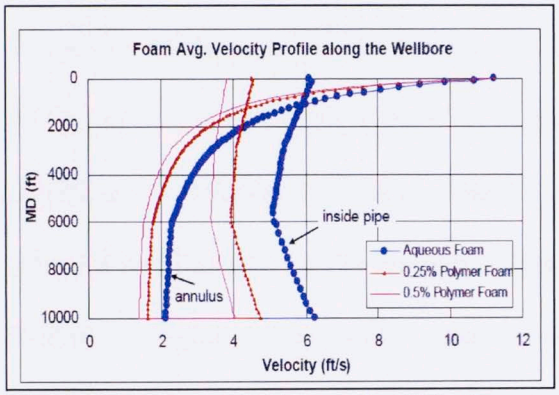

Fig. 3.5 Average velocity vs. depth in three-segment well (After Chen 2005)

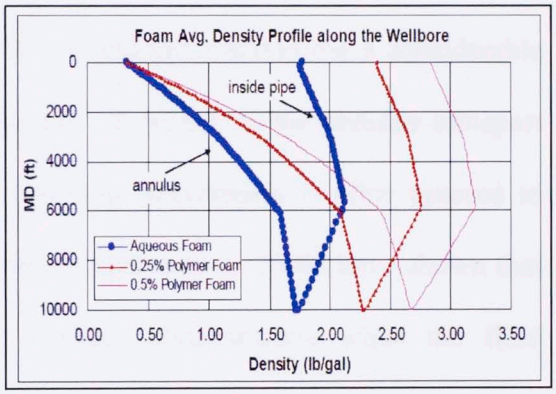

Fig. 3.6 Average density vs. depth in three-segment well (After Chen 2005)

3.3 Modeling of Cuttings Transport with Foam

Although a number of studies (Martins et al. 1998; Ozbayoglu 2002; Li 2004; Chen 2005; Duan et al. 2008) have been conducted to develop the steady-state cuttings transport models, very limited investigations have been performed to model transient cuttings transport in inclined and horizontal wells. Since foam is compressible fluid,

developing cuttings transport model for foam fluid is more challenging than modeling for conventional fluid.

Generally, as drilling progresses, distribution of cuttings in the wellbore varies with time because of the change in rate of penetration, foam flow rate, water/gas influx and other parameters. Hence, the application of steady state models can result in inaccurate prediction of cuttings concentration and pressure profiles in the wellbore. When drilling starts, it takes some time for the cuttings to reach the surface from the bottom of hole. Predicting ECD and pressure profile becomes quite necessary during those transient times because of the necessity of maintaining the bottom-hole pressure within the operating pressure window. Moreover, drillpipe rotation has a considerable impact on the cuttings distribution in the annulus. However, in the cuttings transport modeling, the effect of drillpipe rotation on cuttings distribution is often ignored to reduce the complexity of the models. Experiments (Duan et al. 2008) have shown that drillpipe rotation substantially reduces the cuttings concentration when the fluid velocity is low. However, when axial velocity of fluid is high, the effect of drillpipe rotation on the cuttings concentration is minimal.

Despite its low density, foam poses no problem for the cuttings transport in vertical wells. This is because of its high viscosity. Foam flow velocities as low as 80 ft/min was reported to be used successfully in drilling vertical wells. However, significant variation in foam properties along the wellbore has made hydraulic modeling difficult. In horizontal and inclined wells, hydraulic modeling is more complex than in vertical wells. Since the particle settling is perpendicular to the directions of fluid flow, cuttings tend to settle on the low-side of a horizontal or inclined wellbore due to gravity.

Therefore, high viscosity and high velocity is required for effective cuttings removal in horizontal and inclined wells.

In the past, limited flow loop studies (Okpobiri and Ikoku 1983; Ozbayoglu 2002; Capo 2002) were performed on foam to develop mechanistic cutting transport models. Okpobiri and Ikoku (1983) studied cuttings transport under low pressure and ambient temperature conditions in a 28-ft vertical annulus. A semi-empirical correlation was developed to determine the increase in friction pressure losses due to the presence of cuttings in the wellbore. The correlation was used to develop a model to determine the minimum volumetric requirement for foam drilling. They found that the volumetric requirement increases considerably with the increase in particle size; however, only minor increase in volumetric requirement is needed as the penetration rate increases. Later, Owayed (1997) improved Okpobiri and Ikoku's model to account for water-influx in the hydraulic calculation.

Iyoho et al. (1988) developed the new material balance (NMB) model to generate profiles of hole-cleaning parameters in vertical and near vertical sections of wellbores. The model calculates particle velocity and concentrations profiles by solving a set of finite-difference equations representing material transport along the wellbore. The general equation for convective transport model is expressed as:

$$\frac{\partial c_s}{\partial t} = -\frac{\partial (c_s v_s)}{\partial x} \pm F \tag{3.23}$$

where, F represents the influx coming from the formation, c_s is the solid particle concentration and v_s is the particle settling velocity.

Ityokumbul (1994) used the sedimentation-dispersion model to describe the transport of solids in three phase slurry bubble column. The model represents the flux of solids concentration which uses a Fickian equation of the form:

$$\frac{\partial c_s}{\partial t} + (v_l - v_s)\frac{\partial c_s}{\partial z} - E\frac{\partial^2 c_s}{\partial z^2} = 0 \tag{3.24}$$

where, v_l is the carrier liquid velocity and E is the particle dispersion coefficient. At steady state, the Eq. (3.24) reduces to:

$$(v_l - v_s)\frac{\partial c_s}{\partial z} - E\frac{\partial^2 c_s}{\partial z^2} = 0 \tag{3.25}$$

The solution for the above equation is expressed as:

$$c_s = A_1 + A_2 \exp\left(\frac{(v_l - v_s)z}{E}\right) \tag{3.26}$$

Boundary conditions are given by:

$$(v_l - v_s)c_s - E\frac{\partial c_s}{\partial z} = v_l c_s^f; \qquad z = 0 \tag{3.27a}$$

$$\frac{\partial c_s}{\partial z} = 0, \qquad z = l \tag{3.27b}$$

where, c_s^f is the feed solid concentration. Application of boundary condition results in a steady state solution for solid concentration given by:

$$c_s = c_s^f + \frac{v_s c_s}{v_l} \quad or \quad c_s = \frac{c_s^f v_l}{(v_l - v_s)} \tag{3.28}$$

The solution is constant and independent of the dispersion coefficient for the solids in the column. Finally, Ityokumbul proposed the use of Eisenthal-Cornish-Bowden (1974) method to determine the particle settling velocity from Eq. (3.28).

Carmichael (1995) showed that, besides the solution represented by constant value of particle concentration, axial variation in solid particle concentration during

transport in vertical column is also a valid solution for the model. Applying Eq. (3.27a) for the boundary condition at the outlet:

$$uc_s - E\frac{\partial c_s}{\partial z} = v_l c_s^f \;; \qquad z = l \tag{3.29}$$

Left hand side represents flux of concentration c_p in the reactor at $z = l$, while right hand side represents the flux downstream at $z = l_+$. Assuming particle settling velocity is greater than liquid velocity, net upward flux will be zero at steady state. The Eq. (3.29) reduces to:

$$(v_l - v_s)c_s - E\frac{\partial c_s}{\partial z} = 0 \tag{3.30}$$

The solution for concentration is given by:

$$c_s = A_2 \exp\left(\frac{(v_l - v_s)z}{E}\right) \tag{3.31}$$

The solution shows that there is an upward diffusion of particles which is offset by the settling of particle. As a result, c_s decreases exponentially along the length of column. The study also showed that the boundary conditions for solids concentration (Ityokumbul, 1994) may become invalid for the finite values of particle settling velocity. From Eq. (3.28), it can be deduced that if v_s is positive, $c_s > c_s^f$; which means that solid particles are retained in the column to maintain this concentration. On the other hand, if v_s is less than zero, $c_s < c_s^f$; which means that particles are removed with faster rate at the boundary to maintain this concentration. In both these cases, boundary condition $\frac{\partial c_s}{\partial z} = 0$ is not valid. Boundary condition is correct only if $v_s = 0$ or when the axial dispersion becomes infinite. According to Carmichael, the boundary conditions at the outlet depend strongly on the design and operation of the outlet.

Following Ityokumbul (1994), Civan (1996) developed the model for cuttings transport during upward flow of drilling fluid in vertical wells.

$$\frac{\partial c_s}{\partial t} + (v_l - v_s)\frac{\partial c_s}{\partial z} - E\frac{\partial^2 c_s}{\partial z^2} + \dot{q} = 0 \tag{3.32}$$

where, $\dot{q}$ is the rate of deposition of particles over the well surface. Particle settling velocity can be estimated using stokes law. Boundary conditions can be set up from Eq. (3.27). Initial condition is given by Civan (2007) as:

$$c_s = c_{s0}(z), \qquad 0 \le z \le l, \quad t = 0 \tag{3.33}$$

Based on their experimental study, Martins et al. (1998) developed empirical model to predict bed height and pressure loss in the annulus during foam drilling. Foam flow tests were performed with two different gas and liquid injection rates and foam quality was varied from 60% to 90%. The model predicts cuttings transport performance in horizontal and inclined wells. The dimensionless parameters chosen to represent the carrying capacity were defined as "relative height" and "bed erosion capacity". The model presents the relative bed height as a function of either foam quality or generalized Reynolds number.

$$\frac{h}{D_0} = a - b\Gamma^c \tag{3.34}$$

$$\frac{h}{D_0} = c - dN_{re}^e n^f \tag{3.35}$$

where, a, b, c, d, e, f are the regression coefficients. Γ and N_{Re} are the foam quality and the generalized Reynolds number respectively.

Cuttings transport modeling in horizontal and inclined wells is very difficult. Cho et al. (2000) proposed a three-layer cuttings transport model for horizontal and inclined wellbores. The model predicts cuttings transport mechanism. It considers the formation

of three layers: i) stationary bed; ii) moving bed layer above it; and iii) heterogeneous suspension layer at the top. The model predictions including cuttings bed area were compared with previous experimental data and showed a good agreement with the measurements.

Hole inclination is one of the key factors that affects hole cleaning in inclined wells. Ozbayoglu (2002) focused his flow loop experiments on cuttings transport in horizontal and highly-inclined annuli. The ranges for the experimental parameters were: 70 to 90° of inclination; 1 to 16 ft/s average annular velocities; 20 to 90 ft/hr simulated rates of penetration; and 70 to 90% foam qualities. Based on experimental observation, it was proposed that foam cuttings transport can be modeled as flow of three layers of different fluids with distinct properties. The schematic view is shown in Fig. 3.7. The model assumes: Layer I consists of foam flow; Layer II consists of foam flow along with cuttings; and Layer III consists of stationary layer dominated by cuttings. In order to formulate the numerical model, the wellbore is divided into number of segments where each segment has uniform properties. Change in properties for every segment is calculated by using PVT behavior of foam (i.e. equation of state of foam). The model predicts bed height and pressure drop.

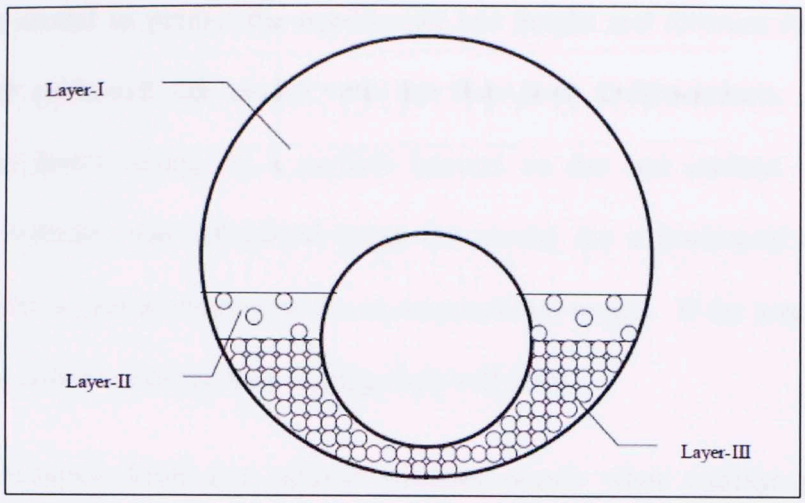

Fig. 3.7 Schematic of three-layered model (Ozbayoglu 2002)

Liquid and gas influxes can significantly change properties of foam in the annulus and subsequently hydraulics and hole cleaning. Li (2004) developed a one dimensional, two-phase mechanistic cuttings transport model for foam flow in horizontal wells. The model assumes uniform cuttings size and complete mixing of the influx with the foam. The model is solved numerically to predict cuttings bed height as a function of drilling rate, gas and liquid injection rates, liquid/gas influx and bore-hole geometry.

Temperature and pressure in the wellbore have strong impact on foam properties. As a result, they can influence hole cleaning performance of foam. Chen (2005) carried out experimental study on foam cuttings transport under high-pressure high-temperature conditions. The study was conducted using a 73-ft long flow loop that has 5.7-in × 3.5-in concentric horizontal annulus. Experiments were carried out at different pressures (100-400 psi) and temperatures (80°F to 170°F). Foam qualities and velocity were varied from 70% to 90% and 2 to 6 ft/s, respectively. Chen (2005) proposed a

mechanistic model to predict the equilibrium bed height and pressure loss along the annulus and calibrated the model with the flow loop measurements. The model analyses the forces acting on a particle located on the bed surface. Critical re-suspension velocity was calculated using the model for a horizontal annulus and compared with actual measurement for an assumed bed height. If the mean velocity is less than the critical velocity, then cuttings bed will form.

Slip between foam and cuttings particles occurs when cuttings particles are suspended in the foam. Kuru and Osunde (2006) developed a two-layer transient model for cuttings transport with foam in inclined wells. The model accounts for the slip between cuttings and foam. The upper-layer consists of foam with suspended cuttings and lower-layer comprises of cuttings bed either stationary or moving are considered in their analyses. Combining the continuity and momentum equations along with water and gas influx rate equations, a numerical model was formulated in discrete form. The model gives the pressure distribution in inclined wellbores.

Pipe rotation has a significant effect on cuttings concentration in horizontal eccentric annulus and subsequently hole-cleaning and pressure loss. Duan et al. (2008) carried out the experiments with a similar set-up and operating conditions as that of Chen (2005). Main difference is that Duan et al. performed the experiments in an eccentric annulus having drill-pipe rotation speeds varying from 0 to 120 RPM. It was inferred that pipe-rotation causes a significant reduction in concentration of cuttings in horizontal eccentric annulus resulting in low friction pressure loss. They proposed a cuttings-transport model to predict the equilibrium bed-height and pressure loss and the model was calibrated with the experimental measurements. An empirical correlation is

developed to determine the critical pressure drop as a function of foam quality, velocity, pipe rotary speeds, wellbore geometry, pressure and temperature. Assuming different bed-heights, actual pressure loss is calculated and compared with the critical pressure loss. If the actual pressure loss is less than critical pressure loss, then cuttings bed will continue to form.

CHAPTER 4: MODELING OF FOAM HYDRAULICS IN THREE-SEGMENT WELLBORES

During underbalanced drilling, predicting foam flow properties including foam density, velocity, quality and pressure has always been a challenge. Unlike conventional drilling fluid, foam is compressible and structured fluid which makes it difficult for hydraulic analysis. Determination of foam rheology along the wellbore is critical for wellbore hydraulic and cuttings transport analysis. Being compressible, foam properties are very sensitive to change in pressure. Foam rheology is strongly affected by pressure, quality and liquid phase rheology. Temperature has major impact on the rheology of liquid. Hence, slight change in pressure or temperature can result in significant variation in foam properties in the wellbore. In this chapter, efforts have been made to model the rheology and hydraulics of foam to investigate the variation in foam properties along the wellbore.

4.1 Conservation Equations

Foam can be treated as a homogenous fluid on a macroscopic scale. From the continuity equation, for steady state flow condition without influx, the rate of mass flowing in is equal to the rate of mass flowing out of a control volume.

$$\rho_1 A_1 v_1 = \rho_2 A_2 v_2 \tag{4.1}$$

According to momentum-conservation equation, total pressure gradient is equal to the sum of frictional pressure gradient, hydrostatic pressure gradient and acceleration pressure gradient.

$$\left(\frac{dP}{dL}\right)_t = \left(\frac{dP}{dL}\right)_h + \left(\frac{dP}{dL}\right)_f + \left(\frac{dP}{dL}\right)_a \tag{4.2}$$

For steady isothermal flow, it can be written as:

$$\frac{dP}{dL} + \rho_f g \cos\alpha + \frac{f\rho_f v^2}{2d_{hyd}} + \frac{\beta\rho_f v dv}{dL} = 0 \tag{4.3}$$

where, β is the momentum correction factor which depends on shape of the velocity profile and assumed to be unity in this case. d_{hyd} is the hydraulic diameter of the annulus. α is the inclination angle measured from vertical. Since difference in fluid velocity between adjacent grids is marginal, the acceleration pressure gradient can be neglected in foam flow.

4.2 Rheological Model

Rheological modeling is necessary to predict flow behavior of foam as a function of quality and base liquid viscosity. The accuracy of foam hydraulic models predominantly depends on the precision of foam rheology model. Chen et al. (2005) conducted rheological investigation on polymer-thickened foam using a specifically designed flow-through rotation viscometer and pipe viscometers. Polymer (Hydroxyethylcellulose) concentration was varied from 0 to 0.5%. Both types of equipment gave consistent rheological parameters. The measured data fitted to the

power-law rheology model. Foam consistency index, K_{foam} and power law exponent, n were correlated to foam quality and base liquid viscosity (Chen et al. 2005).

$$K_{foam}/\mu_L = e^{a.\Gamma^2+b.\Gamma+c} \quad (4.4a)$$

where, a, b and c are given by:

$$a = (-0.533\mu_L^2 + 3.6735\mu_L - 13.546), \quad (4.4b)$$

$$b = (0.8926\mu_L^2 - 6.5877\mu_L + 29.966) \quad (4.4c)$$

$$c = (-0.3435\mu_L^2 + 2.5273\mu_L - 14.218) \quad (4.4d)$$

$$n = -0.45\Gamma + 0.7633 \quad (4.5)$$

The liquid-phase apparent viscosity μ_L is in cp and is measured at a shear rate of $300\,s^{-1}$. The unit of foam consistency index, K_{foam} is in $pa.s^n$. The apparent viscosities of base liquids (0.25% and 0.5% Hydroxyethylcellulose suspensions) at the shear-rate of 300 s^{-1} were 4.7 cp and 8.1 cp. The above correlation is valid when the apparent liquid viscosity at shear rate of 300 s^{-1} is between 1 and 8.1 cp.

4.2.1 Rheological correlations validation with experimental data

Shah and Khade (2004) conducted rheological study on gelled foams. In their investigation, rheological experiments were carried out with guar gel and guar foam fluids at 1,000 psia and temperatures ranging from 100 to 200°F. By analyzing the data at varying foam qualities (from 20 to 80%), empirical correlations were developed to

predict rheology parameters of foam (fluid behavior index, n and consistency index, K) at different qualities and guar gel concentrations. These correlations were used to predict the apparent viscosity of various qualities (20 to 80%) foams. The apparent viscosities obtained from experimental data, Shah and khade's correlation and Chen et al. (2005) correlation are compared. Figure 4.1 shows the comparison of apparent viscosity predictions for 20 lbm/Mgal guar foams at 100°F and 150°F, and shear rate of 511 s^{-1}. It can be seen from these plots that experimental data are in good agreement with the results obtained from the correlations. While Shah and Khade (2004) method predicts apparent viscosity well with the experimental data for all quality foams, Chen et al. (2005) correlation prediction matches well for medium to high quality (> 50%) foams. However, Chen et al. method underpredicts the apparent viscosity of foam at low quality range.

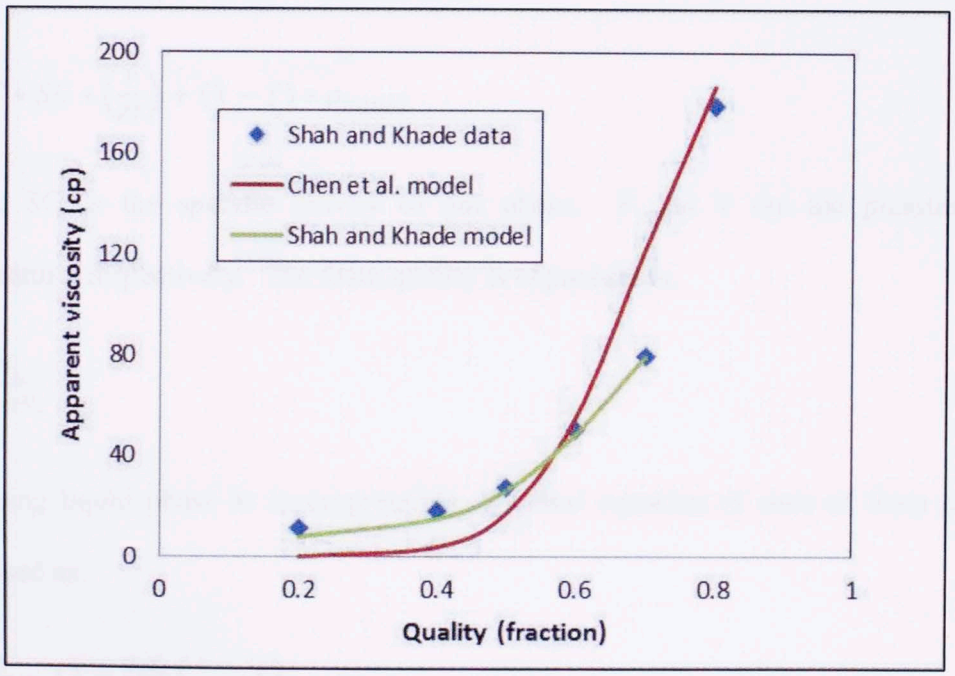

Fig. 4.1 Comparison of apparent viscosity for 20 lbm/Mgal guar foam at 511 s^{-1} and 100°F

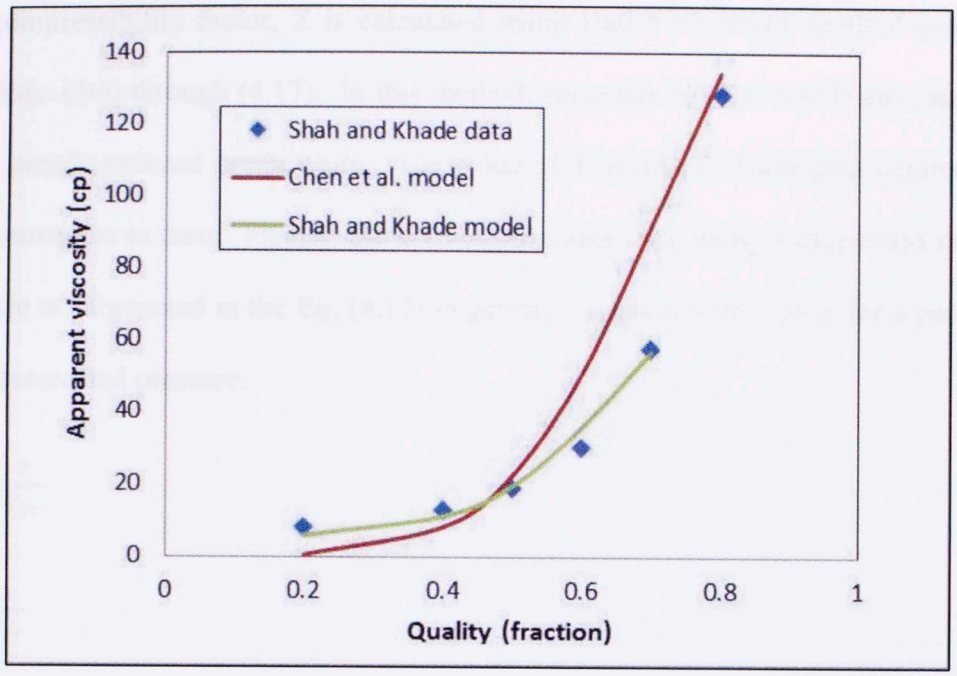

Fig. 4.2 Comparison of apparent viscosity for 20 lbm/Mgal guar foam at 511 s^{-1} and 150°F

Equation of State (EOS), compressibility factor and density of foam are presented below. The density of foam is calculated as:

$$\rho_f = \Gamma * SG * \left(\frac{P}{ZT}\right) + (1 - \Gamma) * \rho_{liquid} \tag{4.6}$$

where, SG is the specific gravity of gas phase. P and T are the pressure and temperature, respectively. The foam quality is expressed as.

$$\Gamma = \frac{V_g}{V_g + V_l} \tag{4.7}$$

Assuming liquid phase as incompressible, the final equation of state of foam can be expressed as:

$$\frac{Z_1 T_1}{P_1}\left(\frac{1}{\Gamma_1} - 1\right) = \frac{Z_2 T_2}{P_2}\left(\frac{1}{\Gamma_2} - 1\right) \tag{4.8}$$

Gas compressibility factor, Z is calculated using Hall-Yarborough method presented from Eqs. (4.9) through (4.17). In this method, constants A, B, C and D are calculated using pseudo-reduced temperature. The value of Y is assumed and then iterated until f(Y) converges to zero. Finally, the convergent value of Y along with pseudo-reduced pressure is substituted in the Eq. (4.17) to get the compressibility factor for a particular temperature and pressure.

$$T_{pr} = \frac{T}{T_{pc}} \tag{4.9}$$

$$t_r = \frac{1}{T_{pr}} \tag{4.10}$$

$$P_{pr} = \frac{P}{P_{pc}} \tag{4.11}$$

$$A = 0.06125 t_r e^{-1.2(1-t_r)^2} \tag{4.12}$$

$$B = t_r(14.76 - 9.76t_r + 4.58t_r^2) \tag{4.13}$$

$$C = t_r(90.7 - 242.2t_r + 42.4t_r^2) \tag{4.14}$$

$$D = 2.18 + 2.82t_r \tag{4.15}$$

$$Y = Assumed$$

$$f(Y) = \frac{Y+Y^2+Y^3-Y^4}{(1-Y)^3} - AP_{pr} - BY^2 + CY^D = 0 \tag{4.16}$$

$$Z = \frac{AP_{pr}}{Y} \tag{4.17}$$

4.3 Hydraulic Model

Though numbers of approaches (Laird 1957; Fredrickson and Bird 1958; Melrose et al. 1958) have been developed to determine the pressure loss for non-Newtonian flow in concentric annulus, the approach based on narrow-slot approximation is widely used because it provides simple analytical solutions.

In the narrow-slot approach, annular flow can be approximated using the equations developed considering a narrow-slot. The slot flow equations are simple to use and give reasonable predictions as long as the radius ratio, $r_1/r_2 > 0.3$. In actual drilling practice, the radius ratio is often greater than 0.3. After applying the narrow-slot method, the average wall shear stress in the annulus for the yield power-law (Herschel–Bulkley) fluid can be determined from the mean flow velocity.

$$\frac{12v}{D_o - D_i} = \frac{(\tau_w - \tau_y)^{\frac{n+1}{n}}}{K^{\frac{1}{n}}\tau_w^2}\left(\frac{3n}{2n+1}\right)\left(\tau_w + \frac{n}{n+1}\tau_y\right) \tag{4.18}$$

Since power-law rheology model best fits drilling foams, the average wall shear stress for power-law fluid in the annulus can be expressed as:

$$\tau_w = K\left(\frac{2n+1}{3n}\right)^n\left(\frac{12v}{D_o - D_i}\right)^n \tag{4.19}$$

During underbalanced drilling, foam flows mostly under laminar conditions. Hence, pressure loss can be calculated directly from the wall-shear stress as:

$$\frac{dP}{dL} = \frac{4\tau_w}{D_o - D_i} \tag{4.20}$$

When the flow is turbulent, the pressure loss is calculated using the Fanning friction factor. The Reynolds number for foam annular flow can be expressed as:

$$Re_{ann} = \frac{8\rho_f v^2}{\tau_w} \tag{4.21}$$

where, τ_w can be determined using Eq. (4.19) for power-law fluids assuming laminar flow. Friction pressure loss can be expressed as:

$$\frac{dP}{dL} = \frac{2f\rho_f v^2}{D_o - D_i} \tag{4.22}$$

where, fanning friction factor (f) is given as:

$$\frac{1}{f^{0.5}} = \frac{4}{n^{0.75}} \log\left[Re_{ann} f^{(1-n/2)}\right] - \frac{0.4}{n^{1.2}} \tag{4.23}$$

4.3.1 Numerical Procedure for Three-Segment Wellbore

A three-segment wellbore is chosen for hydraulic analysis because it represents very common well profile in long radius horizontal wells. For hydraulic analysis, the three wellbore sections (vertical, build-up and horizontal sections) are considered separately. After a kick-off point, well inclination increases at a constant dog-leg angle until it reaches 90° (Fig. 4.1). After this angle, well becomes completely horizontal for the rest of the measured depth.

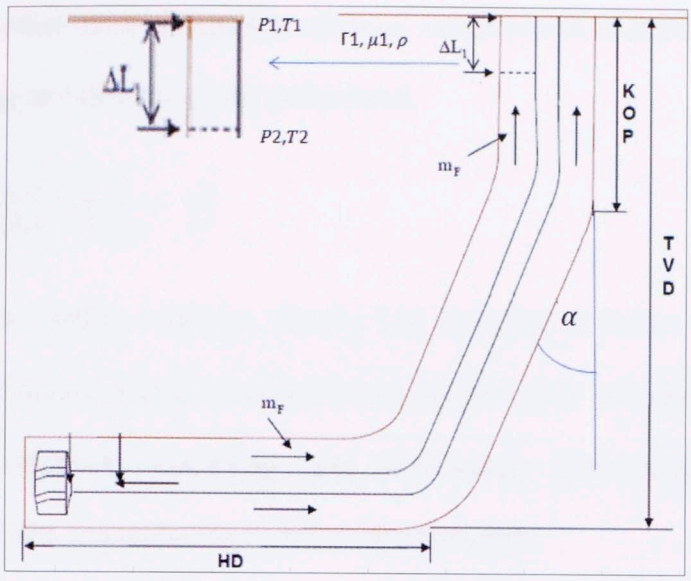

Fig. 4.3 Schematic of foam flow in three-segment wellbore

In order to establish a numerical scheme, the wellbore is sub-divided into 50-ft long grids (wellbore segments). Consequently, the total number of grids is approximately the total measured depth divided by the grid size. Numerical calculation starts from the grid at the top of the annulus and goes down below. The pressure (p_i), temperature(T_i), foam injection rate ($foam\ annular\ velocity, v_i$) and quality ($\Gamma_i$) at Point 1 are known from the surface condition. Based on surface temperature and pressure conditions, compressibility factor (Z_i), foam density (ρ_{fi}) and rheology of fluid at the surface are determined. Temperatures at different points in the wellbore are estimated by knowing the geothermal temperature gradient and surface temperature. Using the steady-state mechanical energy balance equation, pressure (p_{i+1}) at Point 2 is calculated as:

$$\frac{p_{i+1}-p_i}{\Delta L} + \rho_{fi} g \cos\alpha + \frac{f\rho_{fi}v_i^2}{2d_{hyd}} = 0 \qquad (4.24)$$

Subsequently, other flow parameters such as compressibility factor, foam quality, velocity, rheology and density can be determined.

$$\frac{Z_i T_i}{p_i}\left(\frac{1}{\Gamma_i}-1\right)=\frac{Z_{i+1}T_{i+1}}{p_{i+1}}\left(\frac{1}{\Gamma_{i+1}}-1\right) \tag{4.25}$$

Then, foam quality, velocity, density and viscosity at Points 1 and 2 can be averaged to yield the average foam properties in the first grid. Average values of these parameters are calculated iteratively until final steady state values are obtained. Similarly, calculation proceeds downward to all other grids.

4.3.2 Parametric Study

A parametric study on three-segment wellbore hydraulics was conducted using the numerical model presented in Section 4.3.1. The effects of fluid properties, operating parameters and wellbore configuration on pressure and foam hydraulic profiles were studied. Controlled drilling parameters which can be varied to observe their effects on foam hydraulics are back-pressure, gas and liquid injection rate, and well-inclination. To perform a parametric study, a well with 10,000 ft measured depth is considered. Kick-off point starts 5,000 ft from the surface of well and then it builds at the rate of 3° per 100 ft (i.e. dog-leg severity of 3°/100 ft) until the angle reaches 90°. Lengths of wellbore sections are presented in Table 4.1. The hole and drillpipe outer diameters are 9 and 5 inches, respectively. The wellbore geometry is assumed to be uniform. Pure water (without any polymer addition) and air are considered as liquid and gas phases. Hence, base liquid viscosity is 1 cp and gaseous phase specific gravity is 1. Surface fluid temperature is set to be 100°F at the surface, which increases linearly

down-hole with a geothermal gradient of 1.2 °F/100 ft. Other simulation input parameters are presented in Table 4.2. Two cases were studied to examine the impact of back-pressure (200 psi, 400 psi and 600 psi) and surface foam quality on pressure and foam properties profiles and results are presented in the next section.

Table 4.1 Lengths of well sections

Measured Depth	Vertical section	Build-up section	Horizontal section
10000 ft	5000 ft	3000 ft	2000 ft

Table 4.2 Input data for foam hydraulic simulation

Parameters	Values	Unit
Liquid density	8.3	ppg
Liquid Flow rate	2	bbl/min
Drillpipe OD	5	inch
Hole size	9	inch
Depth	10000	ft
Dog-leg angle	3◦	per 100 ft
Rate of Penetration	150	ft/hr
Surface temperature	100	◦F
Temperature Gradient	1.2	◦F/100ft

4.4.3 Results

Case 1: Three simulations were run for different back-pressures of 200, 400 and 600 psi. Liquid-injection rate of 2 bbl/min and gas-injection rate of 23.24 scf/s were kept constant. Figures from 4.2 through 4.6 show pressure, foam quality, velocity, density, apparent viscosity (at shear rate of 100 s^{-1}) profiles in the wellbore.

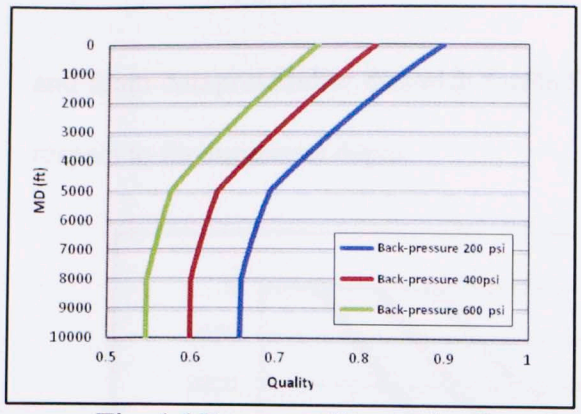

Fig. 4.4 Foam quality vs. depth

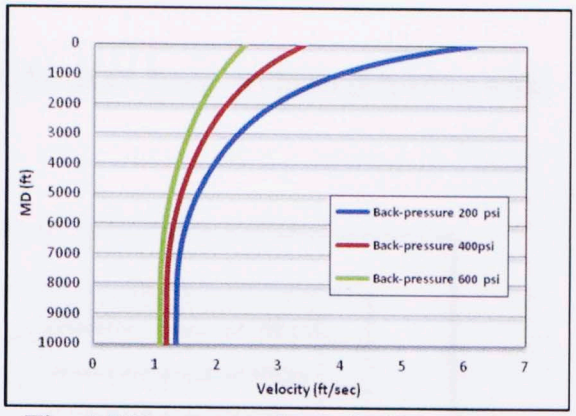

Fig. 4.5 Foam annular velocity vs. depth

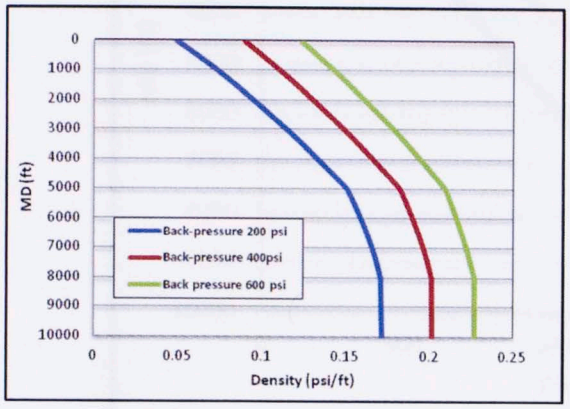

Fig. 4.6 Foam density vs. depth

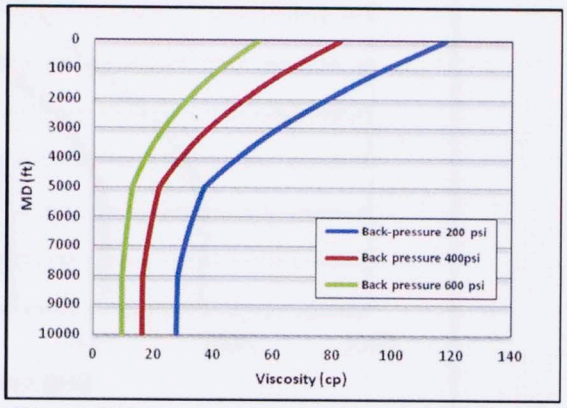

Fig. 4.7 Foam apparent viscosity vs. depth

In the vertical section, pressure, foam density, apparent viscosity, velocity and quality changes significantly with measured depth. Gas being compressible, foam expands significantly in the vertical section where the pressure gradient and foam compressibility are high. In the build-up sections, the variation in pressure and foam properties with measured depth diminishes as the well inclination increases and reaches to the minimum when the well becomes horizontal. Consequently, the contribution of the hydrostatic pressure to the total pressure drop diminishes as the inclination increases and reaches zero when the well becomes horizontal. In the horizontal section, the friction pressure mainly contributes to the total pressure drop. The pressure gradient

and foam compressibility diminish leading to the small change in foam properties with respect to the measured depth.

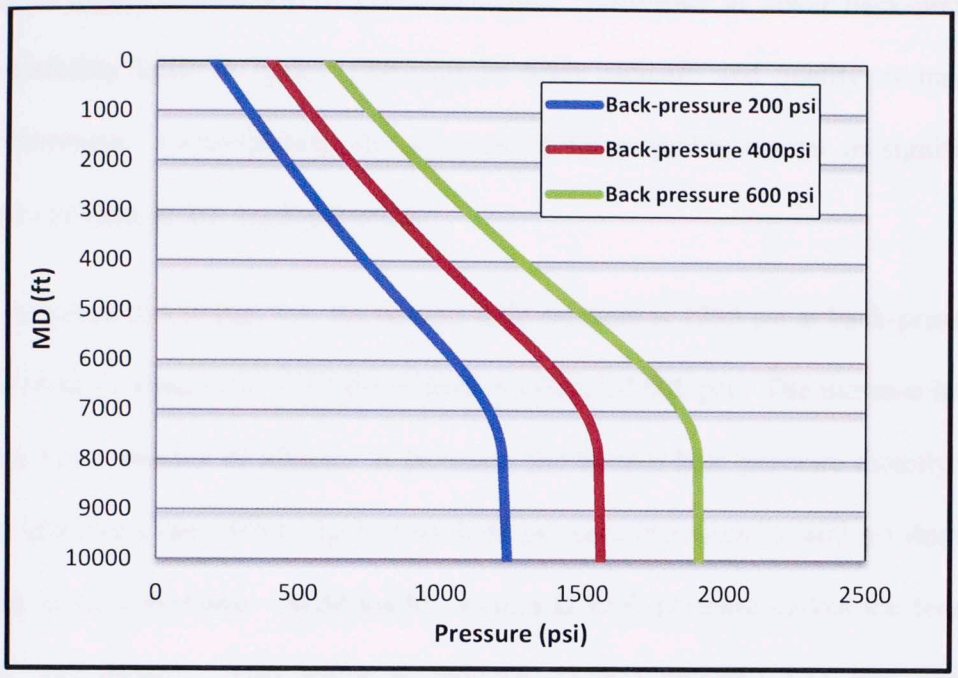

Fig. 4.8 Annular pressure vs. depth

Figures from 4.2 through 4.5 show the effect of back-pressure on the foam-properties. From the plots, it can be noticed that the foam quality, velocity and apparent viscosity throughout the wellbore decrease with the increase in back-pressure. On the other hand, density increases with the increase in back-pressure. Reduction in foam quality in the wellbore is higher at the back-pressure of 200 psi (90% to 65%) as compared to that of 600 psi back-pressure (75% to 54%). Similarly, reduction in velocity is higher at the back-pressure of 200 psi (6 to1.34 ft/s) when compared to the 600 psi back-pressure (2.45 to 1.08 ft/s). Viscosity decreases significantly from 117.8 cp to 28 cp at back-pressure of 200 psi whereas it reduces from 55.2 cp to 9.7 cp at 600 psi back-pressure. The reason for this could be attributed to the inverse relationship

between the pressure and gas compressibility. At high pressure, gas is denser resulting in lower gas compressibility. However, at low pressure, gas compressibility is higher leading to higher contraction of gas with depth. Therefore, at lower back-pressures, compressibility leads to higher reduction in foam velocity and quality as measured depth increases. Consequently, the decrease in foam quality results in significantly reduced viscosity at low back-pressures.

As presented in Fig. 4.6, the bottom-hole pressure is 1235 psi at back-pressure of 200 psi while it reaches to 1912 psi at back-pressure of 600 psi. The increase in back-pressure has a number of effects. It increases the bottom hole pressure directly. This means, ignoring other effects the bottom hole pressure increases by 400 psi due to the increase in back pressure. Additionally, increased back-pressure makes the foam less viscous and denser. This result in reduced friction pressure loss and increased hydrostatic head. However, the impact of hydrostatic pressure dominates the friction effect resulting in higher bottom hole pressure.

Case II: Two simulations were run for different surface foam qualities of 0.8 and 0.9 at back-pressure of 300 psi. Total foam-injection rate was maintained constant at 23.43 scf/s. Figures from 4.7 through 4.11 show the foam quality, density, velocity, apparent viscosity (at shear rate of 100 s^{-1}) and pressure profiles in the three-segment wellbore. The results demonstrate the effect of surface foam quality on foam properties profiles in the wellbore. Figure 4.7 shows significant reduction in foam quality in the wellbore as the surface foam quality decreases. Bottom hole foam quality of 0.73 is expected when the foam quality is 0.9 at the surface. The bottom hole foam quality reduces

significantly (i.e. from 0.73 to 0.5) when the surface foam quality is decreased from 0.9 to 0.8.

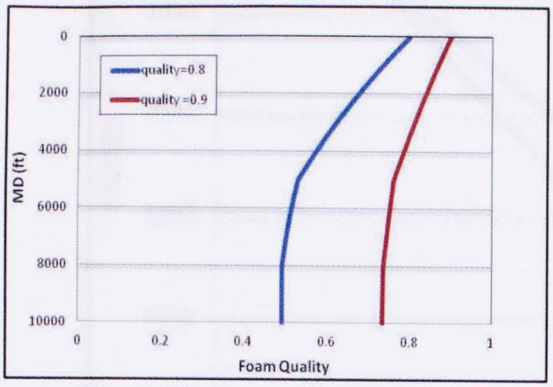

Fig. 4.9 Foam quality vs. depth

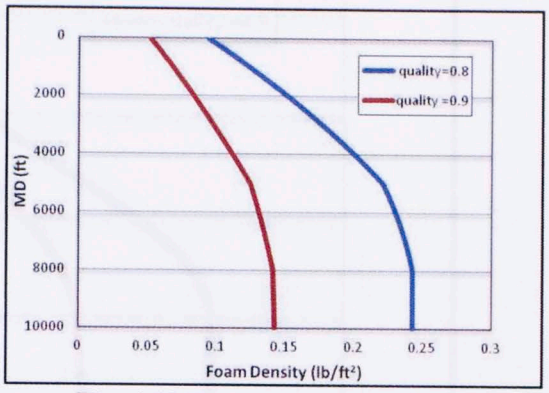

Fig. 4.10 Foam density vs. depth

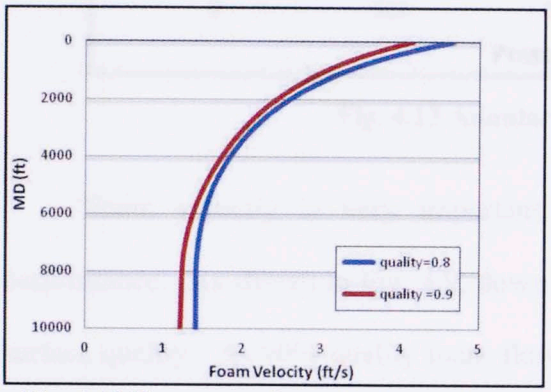

Fig. 4.11 Foam annular velocity vs. depth

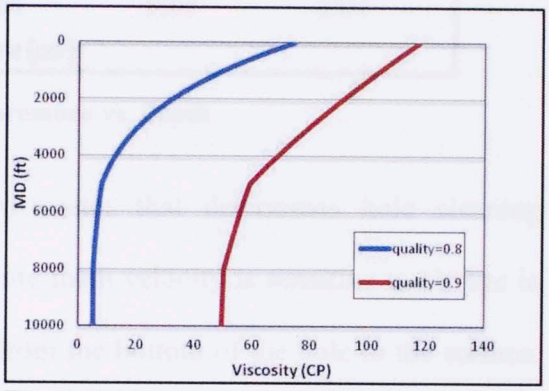

Fig. 4.12 Foam apparent viscosity vs. depth

Furthermore, the bottom hole density is found to be very sensitive to the change in surface quality. Results presented in Fig. 4.8 show significant increase in bottom hole foam density (0.14 psi/ft to 0.24 psi/ft) as surface foam quality reduces from 0.9 to 0.8. This is as a result of the higher hydrostatic pressure gradient at a lower surface foam quality resulting in more compression of gaseous component and hence higher reduction in bottom hole foam quality. The reduction in foam quality has a direct impact on the pressure profile. Figure 4.11 shows the increase in bottom-hole pressure resulting from reduction of surface foam quality.

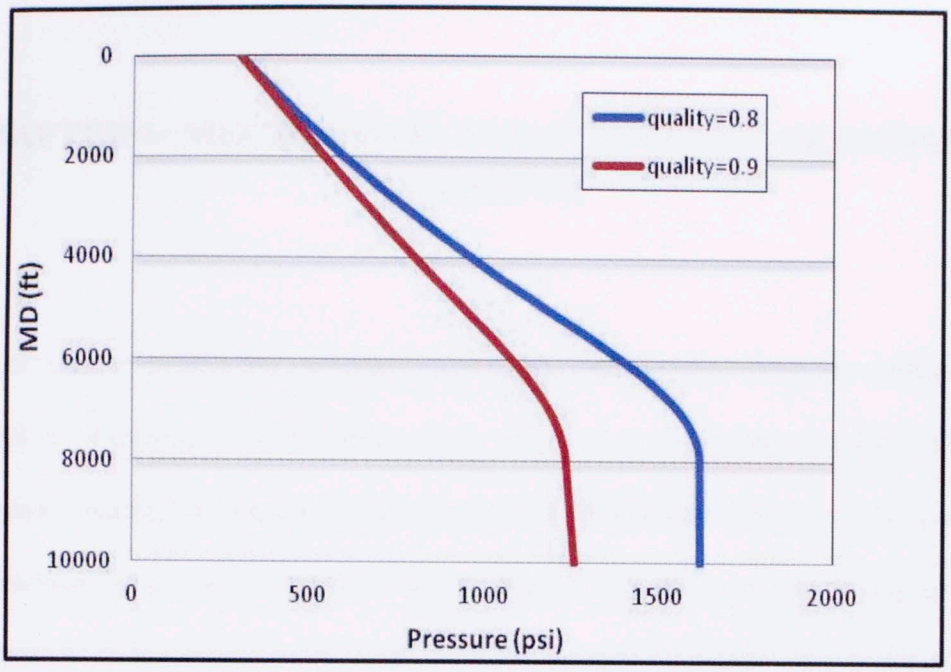

Fig. 4.13 Annular pressure vs. depth

Foam velocity is very important parameter that determines hole cleaning performance. As shown in Fig. 4.9, down hole foam velocity is sensitive to change in surface quality. As 90% quality foam flow from the bottom of the hole to the surface, its velocity increases from 1.2 to 4.2 ft/s. The velocity increase depends on the quality of foam. Results clearly indicate that velocity increase is initially higher for viscous 90% quality foam in horizontal and build-up sections because of expansion due to friction pressure change. However, in the vertical section, velocity increase is higher for 80% quality foam due to increased hydrostatic pressure gradient leading to expansion of foam. Since the contribution of friction pressure loss is little as compared to hydrostatic pressure gradient in the wellbore, overall annular velocity change is higher for 80% quality foam. For 80% quality foam, the velocity increases from 1.4 to 4.7 ft/s as the foam flows from the bottom of the hole to the surface.

CHAPTER 5: MECHANISTIC FOAM CUTTINGS TRANSPORT MODELING

In order to predict the cuttings concentration and pressure along the wellbore, it is essential to understand the theories, which are used to formulate a model and basic assumptions applied in simplifying the formulation. Since foam hydraulics have already been discussed in previous Chapter 4, in this chapter only foam cuttings transport model is presented. In horizontal wells, foam cuttings transport in steady state is described as a flow of layer of two different fluids (stationary bed and moving layer of foam flow). In vertical section, only one layer is assumed. Three different model formulations have been developed to simulate: i) steady state foam cuttings transport in vertical and horizontal wells; and ii) transient cuttings transport.

5.1 Model Hypotheses

The following assumptions are considered in development of mathematical model for foam hydraulics and cuttings transport:

1. Foam is a homogenous compressible fluid described by power law fluid model.
2. Foam is considered as stable fluid and hence, its rheology does not change with time.
3. There is no wall slip during foam flow.
4. Slippage between foam and cuttings is considered.

5. Drill cuttings are considered to be spherical with uniform size.
6. Only convective transport of cuttings by bulk motion of fluid is considered.
7. Transport by diffusion due to concentration gradient is neglected.
8. Under steady state condition, clean foam fluid (without cuttings) is assumed to flow in the upper layer above stationary bed in the deviated section.
9. Rotation effect of drillpipe is not considered.
10. Only steady state water influx is assumed. Water flowing into the wellbore completely commingles with drilling foam.
11. Influx water accelerates to the new mean foam velocity instantaneously.

5.2 Mechanism of Cuttings Transport in Vertical Wells

When cuttings particles suspend in foam, the particles tend to settle due to the gravitational force. Initially, the counter-acting forces including the buoyancy and drag forces become less than the gravitational force. The imbalance of these forces results in particle accelerating and the subsequent increase in its relative velocity (slip velocity). However, with the increase in relative velocity of the particle, the drag force also increases until the net force acting the particle reduces to zero. At this point, the sum of upward forces becomes equal to the sum of downward forces, and the particle reaches its terminal (settling) velocity. The sum of the gravitational and buoyancy forces causing the particle to fall is given by:

$$F_g = \frac{\pi d^3}{6}(\rho_s - \rho_f)g \tag{5.1}$$

The settling of the particle in the fluid results in slippage-opposing drag force, which can be expressed as:

$$F_D = C_D \frac{\rho_f v_s^2}{2} \frac{\pi d^2}{4} \tag{5.2}$$

where, C_D is the drag coefficient, d is the particle diameter and v_s is the slip velocity between fluid and solid particles. Under equilibrium condition, adding gravity, buoyancy and drag force, we get:

$$v_s = \left(\frac{4gd(S_s-1)}{3C_D}\right)^{0.5} \tag{5.3}$$

where, S_s is the density ratio, which is equal to ρ_s/ρ_f. Cuttings density (ρ_s) varies depending on the type of formation rocks being drilled. Different minerals constituting a rock matrix have different densities as shown in Table 5.1. However, cuttings used in the simulation study have a mean density of 2.3 g/cc. Drill cuttings particle size distribution is mainly related to the type of formation rock and drill bits. Generally, for determining particle size, a particle size distribution analysis is performed and the mean diameter (D50) is used to characterize the particle size. D50 is the particle size at which 50 % of sand by weight has passed through the sieve. Using the particle size distribution results from Chen et al. (2005) experimental study, 80% of the cuttings are found to be distributed within a range of 2-4 mm. The sand mean diameter (D50) is 3 mm.

Table 5.1 Common values of matrix density

Solid	Density (g/cc)
Quartz-sand	2.65
Limestone	2.71
Dolomite	2.87
Anhydrite	2.96
Gypsum	2.32

During foam drilling, foam flows up in the annulus and carries the cuttings lagging behind it. The difference in the velocity between the fluid and the particles

depends on the drag coefficient and difference in the density of cuttings and foam. Since foam is a lighter fluid as compared to conventional mud, the difference in the density of cuttings and foam is higher causing a relatively higher slip velocity. However, higher viscosity of foam tends to prevent the slippage of cuttings in the foam and help hole cleaning.

Since power-law rheological model has been used for characterizing foam fluid, the particle Reynolds number for power law fluid can be expressed as:

$$Re_p = \frac{\rho v_s^2}{k\left(\frac{v_s}{d}\right)^n} \tag{5.4}$$

Volumetric flow rate of cuttings generated at the bit is given by:

$$Q_s = \frac{ROP * \pi D_h^2}{4} \tag{5.5}$$

5.3 Cuttings Transport with Foam in Horizontal Wells

As previously discussed, drag force acts directly opposite to the gravitational force and helps in the lifting of particle to a larger extent. However, in the inclined or horizontal wells, drag force acts in the direction of fluid flow which makes an angle to the direction of gravitational force. The drag force has a reduced vertical component; as a result, higher foam velocity is needed to provide the required lifting force for cuttings suspension in inclined wellbore than vertical wells. However, excessive foam velocity is undesirable because of wellbore and casing erosion. Hence, with limited foam velocity, the drilled cuttings tend to deposit on the low-side of the wellbore. Once the cuttings bed is formed in the wellbore, foam flows over the bed in the remaining unblocked annular area (Fig. 5.1).

As can be seen in Fig. 5.1, flow of foam cuttings mixture in steady state can be considered as two layers of different fluids with distinct properties: i) bottom stationary layer with equilibrium cuttings bed, and ii) upper moving layer with negligible cuttings. At the interface, the cuttings roll and bounce just above the surface of the stationary bed.

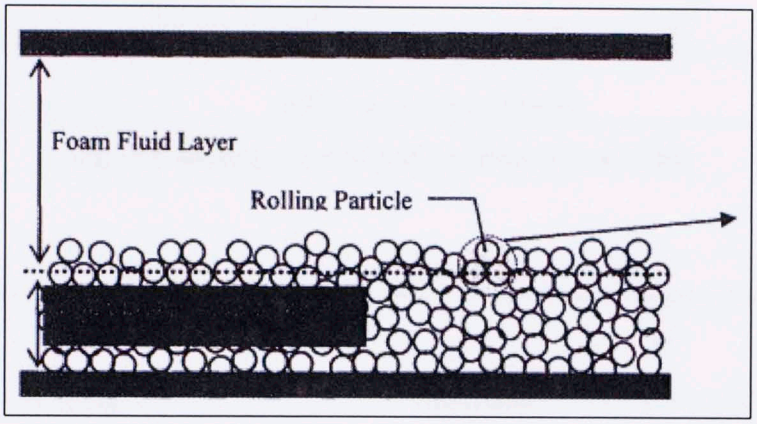

Fig. 5.1 Cuttings transport with foam in horizontal annulus (Chen 2005)

5.3.1 Force Analysis in Particle Transport

The knowledge of forces acting on a single particle can be helpful in the analysis of particle transport and re-suspension. The interaction between particles laying on the surface of the bed (Fig. 5.2) and the foam can be results in momentum transfer, which imposes hydrodynamic forces (drag and lift forces) on the particle in addition to the static forces. The hydrodynamic forces (Fig. 5.3) can be strong enough to initiate a motion to the particle. Therefore, it is very essential to study the details of these forces to understand the behavior and the trajectory of a given bed particle.

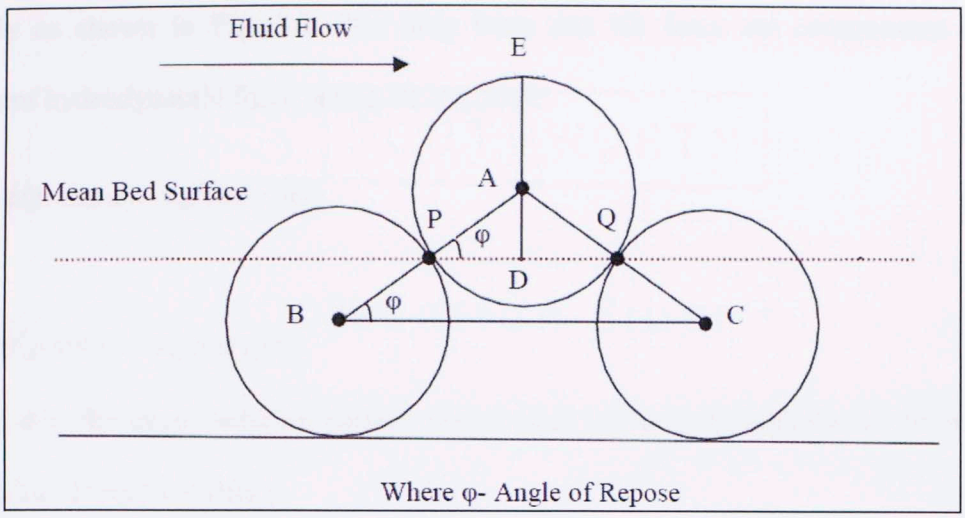

Fig. 5.2 Arrangement of bed particles (Duan 2005)

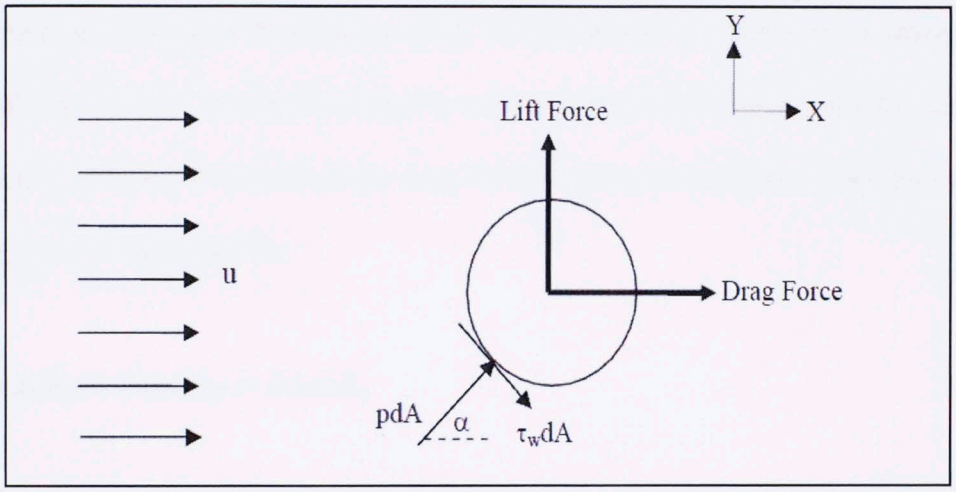

Fig. 5.3 Drag and lift force acting on the surface of a bed particle (Chen 2005)

There are two types of forces which acts on a particle suspended in fluid: i) static forces are gravity and buoyancy; and ii) hydrodynamic forces are forces acting on a particle due to the movement of the particle relative to the fluid. Drag and lift force are the dominant hydrodynamic forces which are experienced when a body moves relative to its surrounding fluid. These forces are the result of pressure and shear stress acting on

a body as shown in Fig. 5.3. The drag force and lift force are components of the resultant hydrodynamic force acting on a particle.

$$F_D = \oint (p \cos\alpha + \tau_w \sin\alpha) dA \tag{5.6}$$

and,

$$F_L = \oint (p \sin\alpha - \tau_w cos\alpha) dA \tag{5.7}$$

where, α is the angle between normal vector (unit vector perpendicular to the particle surface) and local velocity u.

Equations (5.6) and (5.7) are valid for any particle in a fluid. However, the difficulty lies in obtaining the shear stress and pressure distribution on the body surface. For a creeping flow past Newtonian fluid, forces around a sphere were integrated analytically by Stokes. It was found that two-third of the drag force is from the viscous component $\tau_w dA$; and one-third of the drag force is from the pressure component pdA. The drag force is expressed as:

$$F_D = 4\pi\mu u R_p + 2\pi\mu u R_p = 6\pi\mu u R_p \tag{5.8}$$

Drag force is present in all types of flow around a solid bed particle and is mostly superior over other hydrodynamic forces. Lift force on a particle is present only if there is any asymmetry in the flow field. There is no lift force in this case (Fig. 5.3) as the flow is uniform producing no shear gradient along the axis perpendicular to the relative velocity. For complex flows, analytical integration of these forces is challenging; hence, drag and lift coefficients are introduced to calculate these force using empirical correlations. The drag and lift coefficients are defined as:

$$C_D = \frac{F_D}{0.5\rho_F u^2 A} \tag{5.9}$$

$$C_L = \frac{F_L}{0.5\rho_F u^2 A} \tag{5.10}$$

A number of correlations for drag and lift coefficients are available. The correlations have been developed for Newtonian fluids and later extended to the Non-Newtonian fluids. Drag coefficient is a function of shape, size, surface roughness of the particles, fluid properties and flow parameters. Drag coefficient is only a function of the Reynolds number for spherical particles. However, for non-spherical particles, drag coefficient also depends on a term called sphericity, Ψ. Sphericity of the sphere is 1 and it decreases with irregularity. Sphericity is defined as the ratio of the surface area of a sphere having the same volume as the particle to the surface area of the particle. The more irregular or non-spherical the particle, the greater the drag force acting on the particle. In this study, a generalized correlation for drag coefficient of spherical particles presented by White (1991) is used.

$$C_D = \frac{24}{Re_p} + \frac{6}{1+Re_p^{0.5}} + 0.4 \tag{5.11}$$

The above equation for drag coefficient (Eq. 5.11) can be applied for both Newtonian and Non-Newtonian fluids as well as for all the flow regimes including laminar, transitional and turbulent flows. Lift coefficient proposed by El-Samni (1949) for spherical particles is defined as:

$$C_L = 0.09 \qquad (C_L < 0.09) \tag{5.12}$$

$$C_L = 5.82\left(\frac{d}{2u}\frac{du}{dy}/Re_p\right)^{0.5} \qquad (C_L > 0.09) \qquad (5.13)$$

5.3.2 Near-bed Wall-Shear Stress Determination

In an eccentric annulus, cuttings bed influence the distribution of local velocity and local shear stress during foam flow. Fig. 5.4 shows the velocity distribution of a non-Newtonian fluid in concentric and eccentric annulus in the presence of cuttings bed. In general, local fluid velocity varies throughout the annulus with maximum being at zero stress location and minimum near the wall or the bed.

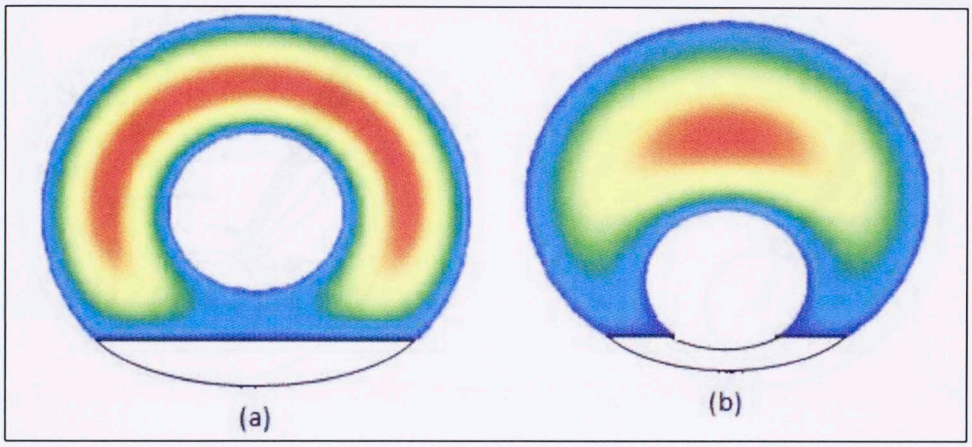

Fig. 5.4 Velocity distribution with cuttings bed in (a) concentric annulus; and (b) eccentric annulus (Aworunse 2012)

In concentric annulus, axial velocity profile remains uniform throughout the annulus because of simple flow geometry. However, when the inner pipe is off-centered or cuttings bed forms at the low-side of the annulus, the velocity profile becomes non-uniform and complex. Analytical solution is not difficult to obtain for eccentric annular flow of non-Newtonian fluids. Luo and Peden (1987) developed an approximate model for flow in eccentric annulus. The eccentric annular flow was

modeled by as an infinite number of concentric annuli with variable outer radius. This procedure has been utilized for determining near-bed wall-shear stress.

Applying this technique, the eccentric annulus is divided into series of sectors of concentric annulus having an angle of $\Delta\theta$ (Fig. 5.5). This procedure generates sectors of concentric annuli with different hydraulic diameter and different flow areas. From the continuity equation, the total flow rate across the annulus is the sum of the flow rates in the sectors. However, the pressure gradient across each sector is same irrespective of the flow rate and geometric variations.

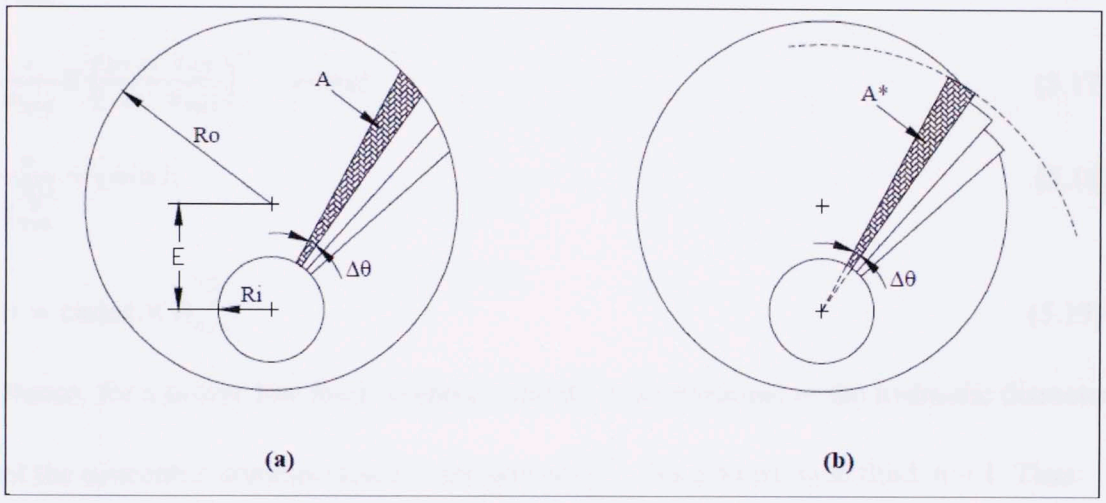

Fig. 5.5 Flow geometries: a) eccentric annulus; and b) equivalent annulus with series of concentric annuli (Ahmed and Miska 2009)

To derive the relationship between local velocity in each concentric sector and the geometric parameters, a constant pressure gradient is assumed.

$$\frac{\Delta P}{L} = constant$$

Pressure gradient due to friction in a cylindrical flow can be expressed as:

$$\frac{\Delta P}{L} = \frac{4\tau_w}{D_{hyd}} \tag{5.14}$$

The average wall shear stress for power law fluid flowing in a concentric annulus under laminar flow condition can be expressed as:

$$\tau_w = K\left(\frac{2n+1}{3n}\frac{12v}{D_{hyd}}\right)^n \tag{5.15}$$

where, D_{hyd} is the hydraulic diameter of concentric annulus and v is the average velocity. From Eqs. (5.14) and (5.15), we get:

$$\frac{4\tau_w}{D_{hyd}} = constant \tag{5.16}$$

$$\frac{4}{D_{hyd}} K\left(\frac{2n+1}{3n}\frac{12v}{D_{hyd}}\right)^n = const. \tag{5.17}$$

$$\frac{v}{D_{hyd}^{\frac{n+1}{n}}} = const. \tag{5.18}$$

$$v = const. \times D_{hyd}^{\frac{n+1}{n}} \tag{5.19}$$

Hence, for a power law fluid, average velocity is proportional to the hydraulic diameter of the concentric annulus raised to the power $\frac{n+1}{n}$. For a Newtonian fluid, n = 1. Thus:

$$v/D_{hyd}^2 = const. \tag{5.20}$$

$$v = const. \times D_{hyd}^2 \tag{5.21}$$

Hence, for Newtonian fluid, average velocity is proportional to the square of hydraulic diameter of the concentric annulus.

Example case:

We divided the eccentric annulus into concentric sectors of angle 5° each. Area of a sector can be expressed as:

$$A_i = 3.1415 * ((R - e\cos(\theta_i))^2 - r^2) \times {}^{5^\circ}/_{360^\circ} \tag{5.22}$$

where, θ_i is the total angle subtended by the sector (Fig. 5.6). Since average velocity in a sector is proportional to hydraulic diameter raised to the power $\frac{n+1}{n}$ as shown in Eq. (5.19). Therefore, the flow rate through the sector:

$$Q_i = v_i \times A_i = const. \times D_{hyd}^{\frac{n+1}{n}} A_i \tag{5.23}$$

Total flow rate in the annulus can be expressed as sum of the flow rates of each sector:

$$Q_{total} = \sum v_i \times A_i = const. \times \sum D_{hyd}^{\frac{n+1}{n}} A_i \tag{5.24}$$

Hence, the constant can be determined by:

$$const. = {}^{Q_{total}}\Big/_{\sum D_{hyd}^{\frac{n+1}{n}} A_i} \tag{5.25}$$

Using the value of the above constant from Eq. (5.25) and substituting back in the Eq. (5.19), we get the local velocity of sector near bed surface:

$$v_{bed} = {}^{Q_{total}}\Big/_{\sum D_{hyd}^{\frac{n+1}{n}} A_i} \times D_{hyd}^{\frac{n+1}{n}} \tag{5.26}$$

Knowing the area (A_{f-bed}) and perimeter (S_{f-bed}) of concentric sector near bed, hydraulic diameter can be calculated as:

$$D_{hyd,bed} = {}^{4A_{f-bed}}\Big/_{S_{f-bed}} \tag{5.27}$$

Using local velocity (Eq. 5.26) and the hydraulic diameter (Eq. 5.27) of concentric sector near the bed, wall-shear stress close to bed can be obtained:

$$\tau_w = K(G(Z,n))^n \left(\frac{8v_{bed}}{D_{hyd,bed}}\right)^n \tag{5.28}$$

where, Geometry factor $G(Z,n)$ is calculated by (Fredrickson and Bird 1958):

$$G(Z,n) = \left[\frac{(3-Z)n+1}{(4-Z)n}\right]\left[1+\frac{Z}{2}\right] \tag{5.29}$$

When the dummy variable Z=0, that is pipe flow, and if Z=1, it reduces to the approximate solution of narrow annular flow. For different combination of diameter ratio (κ) and fluid behavior index (n), the dummy variable Z can be approximated by:

$$Z = 1 - \left(1 - \left(\frac{D_i}{D_o}\right)^Y\right)^Y \tag{5.30}$$

$$Y = 0.37n^{-0.14} \tag{5.31}$$

5.3.3 Near- bed Velocity Profile

As shown in Fig 5.3, the hydrodynamic forces acting on the bed particle depend on the local fluid velocity. Therefore, in order to estimate the drag and lift forces, it is necessary to develop a model to predict the local velocity near the bed. For laminar flow of power law fluid in eccentric annulus, the local velocity profile can be determined analytically using the narrow-slot approximate technique presented in Fig. 5.6. According to this technique, the location of centre position (i.e. zero stress locations) in eccentric annulus can be expressed as (Vaughn 1965):

$$\frac{h}{2} = \lambda = \frac{(c+e\cos\theta)}{2} \tag{5.32}$$

Assuming shear stress varying linearly with distance from the wellbore wall to center position, the shear stress distribution in the annular space can be expressed as:

$$\tau = \frac{\tau_w}{h/2}(y - \lambda) \tag{5.33}$$

where, λ is the value of y at which $\tau = 0$, yields the following integral equation:

$$\int_0^u du = \left(\frac{\tau_w}{K\frac{h}{2}}\right)^{1/n} \int_0^y (\lambda - y)^{1/n} dy, \quad y < \lambda \tag{5.34}$$

$$\int_0^u du = \left(\frac{\tau_w}{K\frac{h}{2}}\right)^{1/n} \int_0^y (y - \lambda)^{1/n} dy, \quad y > \lambda \tag{5.35}$$

Hence, the velocity profile equations can be written as:

$$u = \frac{n}{n+1}\left(\frac{\tau_w}{K}\right)^{1/n}\left(\frac{h}{2}\right)\left[1 - \left(1 - \frac{2y}{h}\right)^{\frac{1+n}{n}}\right], \quad y < \lambda \tag{5.36}$$

$$u = \frac{n}{n+1}\left(\frac{\tau_w}{K}\right)^{1/n}\left(\frac{h}{2}\right)\left[1 - \left(\frac{2y}{h} - 1\right)^{\frac{1+n}{n}}\right], \quad y > \lambda \tag{5.37}$$

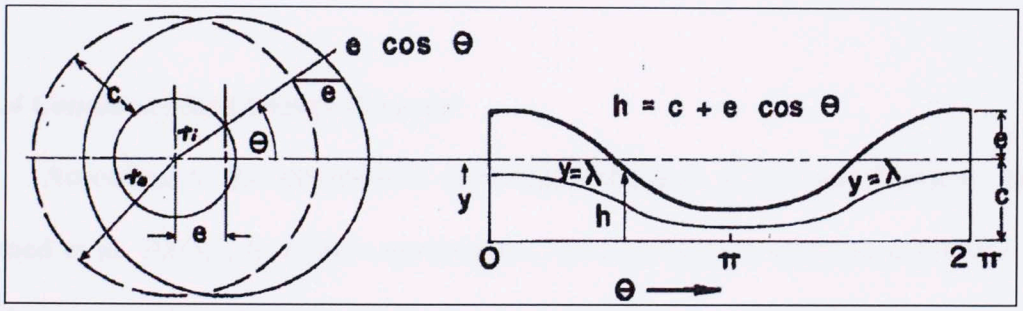

Fig. 5.6 Geometric parameters in eccentric annulus (Vaughn 1965)

Though the above equations are developed for the condition when there are no cuttings deposited in eccentric annulus, it is still valid for the annulus where negligible cuttings get deposited. If we assume that the stationary cuttings bed does not significantly change the velocity profile of foam flow in eccentric annulus, it is possible

to obtain the approximate local velocity at the centre of bed particle. The distance between the centre of the particle and cuttings bed surface can be expressed as:

$$y = \frac{d}{2} sin\varphi \tag{5.38}$$

where, φ is the angle of repose as shown in Fig. 5.2.

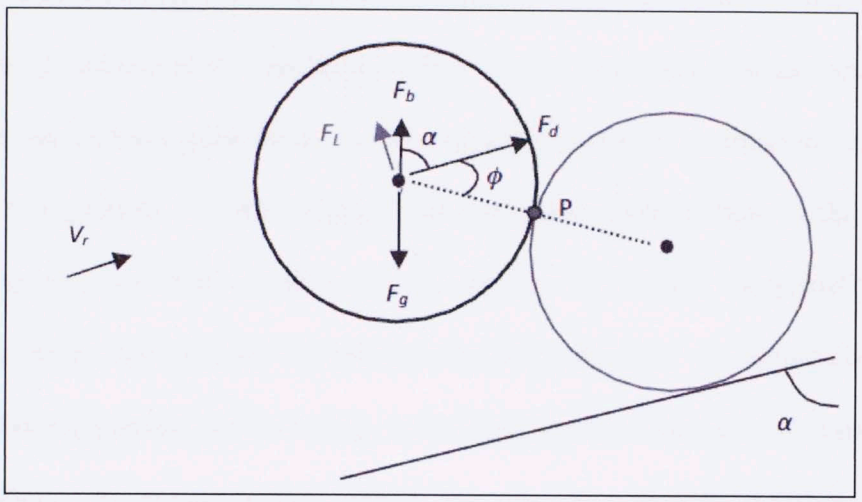

Fig. 5.7 Forces acting on a single cuttings bed particle (Duan 2005)

5.3.4 Conditions for Cuttings Removal

According to the mechanistic modeling techniques (Clark and Bickham 1994; Ahmed et al. 2003c), to initiate movement of bed particles in inclined and horizontal wellbores, net lifting force or net rotating torque acting on a single bed particle should be greater than zero. The forces which contribute to the net lifting or net moment balance are drag and lift forces, force of gravity and buoyancy.

Particle lifting from cuttings bed generally occurs in the vertical or near vertical wells. For lifting to take place, the net force acting on a bed particle in the direction

normal to the bed plane should be positive. Applying force balance, the net lifting force can be obtained.

$$F_{net} = \frac{\pi}{2} d^2 \rho_f \left(\frac{C_L u^2}{4} - \frac{d sin\alpha (s-1) g}{3} \right) \tag{5.39}$$

where, α is the angle of inclination measured from vertical.

As inclination angle increases, net lifting force diminishes and bed particles begin to roll over the surface of the bed before lifting occurs, then the net torque acting on the particle at the contact point between two adjacent particles determines the state of motion of the particle. In the inclined and horizontal wells, rolling is the dominant transport mechanism that occurs over the surface of a bed. Especially at high inclination angles, the particles roll and bounce along the bed. A contact point "P" of two neighboring particle shown in Fig. 5.7 is considered as the axis of rotation during particle rolling. To initiate particle rolling, the net torque must be positive (i.e. in the rolling direction). Hence, applying angular momentum balance, the rolling condition can be mathematically described as:

$$\tau_P = \frac{d}{2} (F_D \sin\varphi + F_L \cos\varphi - W \sin(\alpha + \varphi)) > 0 \tag{5.40}$$

$$\tau_P = \frac{\pi d^3 \rho_f}{4} \left(\frac{C_D \sin\varphi + C_L \cos\varphi}{4} u^2 - \frac{dg(s-1)\sin(\varphi+\alpha)}{3} \right) > 0 \tag{5.41}$$

5.3.5 Procedure for Calculating Equilibrium Bed Height

The calculation of equilibrium bed height is dependent on the foam rheological properties and drilling parameters. Steps for calculating equilibrium bed height in the wellbore are given below:

Step 1. Divide the wellbore into small computational segments.

Step 2. Assume initially clean wellbore without cuttings and calculate foam properties in each segment.

Step 3. Gradually increase the bed height and use Eq. (5.27) to calculate the hydraulic diameter of a concentric sector near the bed.

Step 4. Knowing the local sector velocity near the bed from Eq. (5.26) and hydraulic diameter for the concentric sector close to the bed, estimate the near-bed wall shear stress in the eccentric annulus.

Step 5. Using the local wall shear stress in Eqs. 5.36 and 5.37 presented in Section 5.3.3, calculate the local velocity at the centre of a particle, which is laying on the bed surface.

Step 6. Knowing the local velocity and velocity-gradient, calculate the drag and lift forces acting on the particle. Use Eq. (5.41) to estimate the torque imposed on the particle.

Step 7. If the resultant torque is greater than zero, it means that the cuttings deposition have reached the equilibrium bed height. If the torque is less than zero, increase the bed height and repeat Steps 3 to 7, until the resultant torque becomes greater than zero.

The final equilibrium bed height will vary depending upon the location of the computational segment in the wellbore, fluid properties and drilling parameters.

5.4 Transient Cuttings Transport Model

When drilling is started, cuttings generated at the bottom of the annulus start moving together with the drilling fluid. However, carry capacity of the fluid is limited and some of the particles deposit or accumulate in the annulus. As a result, the cuttings concentration increases with time along the wellbore until it reaches the steady state condition. The bottom part of the wellbore is filled with the cuttings first and subsequently the upper sections of wellbore are filled. In build-up and horizontal sections of wellbore, the cuttings deposit in the low-side of the wellbore until the local fluid velocity becomes high enough to reach the critical velocity limit. At the critical velocity, net rotating torque or lift force acting on the cuttings becomes zero and cuttings deposition or accumulation reaches the steady state. Based on this, a new transient cuttings transport model for the three-segment wells has been formulated to investigate real-time accumulation of cuttings and pressure profile in the wellbore. This can help in successful application of foam drilling in depleted reservoirs.

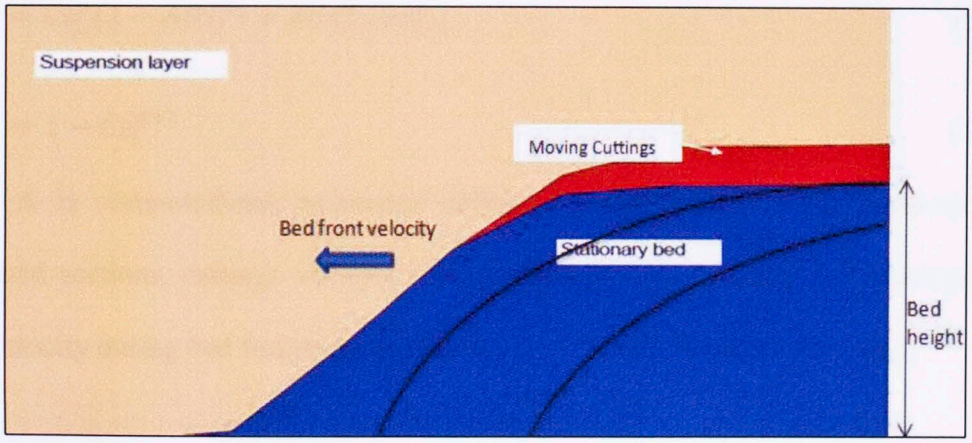

Fig. 5.8 Cuttings bed layer front movement

Equations (5.42a) and (5.42b) are the continuity equations representing conservation of mass for foam and cuttings, respectively:

$$\frac{\partial}{\partial t}(C_f \rho_f) + \frac{\partial}{\partial x}(C_f \rho_f u_f) = s_f \tag{5.42a}$$

$$\frac{\partial}{\partial t}(C_s) + \frac{\partial}{\partial x}(C_s U_s) = 0 \tag{5.42b}$$

The above equations are discretized using backward difference in space and forward difference in time, Hence:

$$\frac{\partial}{\partial x}(Cs_i^n Us_i^n) \cong \frac{Cs_i^n Us_i^n - Cs_{i-1}^n Us_{i-1}^n}{\Delta x} \tag{5.43a}$$

$$\frac{\partial}{\partial t}(Cs_i^n) \cong \frac{Cs_i^{n+1} - Cs_i^n}{\Delta t} \tag{5.43b}$$

Subsequently, the mass conservation equations for cuttings and foam can be expressed in discretized form as:

$$Cs_i^{n+1} = Cs_i^n(1 - AUs_i^n) + ACs_{i-1}^n Us_{i-1}^n \tag{5.44}$$

$$Cf_i^{n+1} = 1 - Cs_i^{n+1} \tag{5.45}$$

where A is computational parameter defined as: $A = \Delta t/\Delta x$. For build-up and horizontal sections, cuttings velocity is same as bed formation rate (i.e. cuttings bed front velocity during bed formation as shown Fig. 5.8), which can be given by:

$$Us_i^{n+1} = \frac{Qs}{A_{bed_i}(1-\emptyset)} \tag{5.46}$$

For vertical section, cuttings transport velocity can be calculated by subtracting slip from foam fluid velocity:

$$Us_i^{n+1} = \frac{V_i}{1-Cs_i^{n+1}} - V_s e^{(-5.9Cs_i^{n+1})} \tag{5.47}$$

where, C_s is the cuttings volume concentration and C_f is the foam volume fraction. $\emptyset$ is the bed porosity. Us is the cuttings velocity. A_{bed} is the area of the bed. V_s is the slip velocity

The following initial and boundary conditions are applied for predicting cuttings concentration profile in wellbore at different time steps until steady state condition establishes.

$$Cs_i^1 = 0;\ i = 2,3,..l \tag{5.48a}$$

$$Us_i^1 = 0;\ i = 2,3,...l \tag{5.48b}$$

$$Cs_1^n = \frac{Q_s}{Q_s+Q_f};\ n = 1,2 \ldots N \tag{5.48c}$$

$$Us_1^n = \frac{Q_s+Q_f}{A_{ann}};\ n = 1,2 \ldots N \tag{5.48d}$$

where,

Cs_i^1 is the initial cuttings concentration in the grid i.

Us_i^1 is the initial cuttings transport velocity in grid i

Cs_1^n is the in-situ cuttings concentration at the bit at any time

Us_1^n is the cuttings velocity at the bit at any time

Q_s is the solid/cuttings flow rate

Q_f is the foam flow rate at the bit

Equations (5.49a) and (5.49b) are conservation of momentum equations for foam and cuttings, respectively.

$$\frac{\partial}{\partial t}(C_f \rho_f u_f) + \frac{\partial}{\partial x}(C_f \rho_f u_f^2) = -C_f g_c \frac{\partial p}{\partial x} - \beta_v (U_f - U_s) - C_f \rho_f g \cos\alpha - f \frac{C_f \rho_f U_f^2}{2D_{hyd}} \quad (5.49a)$$

$$\frac{\partial}{\partial t}(C_s \rho_s u_s) + \frac{\partial}{\partial x}(C_s \rho_s u_s^2) = -C_s g_c \frac{\partial p}{\partial x} + \beta_v (U_f - U_s) - C_s \rho_s g \cos\alpha \quad (5.49b)$$

Here, the frictional pressure drop due to solid effects has been neglected and only the foam fluid friction factor has been considered. Uf is the mean velocity of foam. Adding Equations (5.49a) and (5.49b), and neglecting the pressure variation due to the acceleration effects, the following expression can be obtained:

$$-g_c \frac{\partial p}{\partial x} = (C_f \rho_f g + C_s \rho_s g) \cos\alpha + f \frac{C_f \rho_f U_f^2}{2D_{hyd}} \quad (5.50)$$

Discretizing the above equation by back-ward difference in space:

For vertical section:

$$-g_c \frac{p_i^n - p_{i-1}^n}{\Delta x} = (Cf_i^n \rho_{fi} + Cs_i^n \rho_s) g + f \frac{Cf_i^n \rho_{fi} U_{fi}^2}{2D_{hyd}} \quad (5.51)$$

After cuttings bed formation, cuttings particles move on the bed-surface with the mean velocity of the foam. Consequently, suspended cuttings concentration in upper layer along the build-up and horizontal section is same as the in-situ concentration at the steady-state condition.

$$Uf_i = v_i \quad (5.52a)$$

$$Cr_i^n = 0; \qquad \text{Before bed deposition} \tag{5.52b}$$

$$Cr_i^n = \frac{Q_s}{Q_s+Q_f} = Cv; \qquad \text{After bed depostion} \tag{5.52c}$$

For build-up and horizontal section:

$$-g_c \frac{p_i^n - p_{i-1}^n}{\Delta x} = \left(Cf_i^n \rho_{fi} + Cr_i^n \rho_s\right) g \cos\alpha_i + f \frac{Cf_i^n \rho_{fi} U_{fi}^2}{2D_{hyd}} \tag{5.53}$$

Boundary condition:

$$p_l^n = P_B;\ n = 1,2 \ldots N \tag{5.54a}$$

Initial condition can be obtained by substituting Eq. (5.48a) in (5.53):

$$-g_c \frac{p_i^1 - p_{i-1}^1}{\Delta x} = \rho_{fi}\, g \cos\alpha_i + f \frac{\rho_{fi} u_{fi}^2}{2D_{hyd}} \tag{5.54b}$$

Pressure calculation starts from the surface and goes down to the bottom. Here, P_B denotes the back-pressure at the surface.

Foam mass rate would be affected by the influx of formation fluids represented by the source term s_f. The source term in the Eq. (5.42a) is defined as the mass rate of influx of water, oil and gas from the reservoir due to the drawdown created during the underbalance.

$$s_f = \sum PI_j \times (P_{res} - P) \tag{5.55}$$

5.4.1 Solution Algorithm of Transient Equations

i. Start the calculations from the bottom to surface varying grid index i from 2 to L and repeat the computation for each time step.

ii. Solve Equations (5.44) and (5.45) for concentrations using the initial and boundary conditions.

iii. For every time step, solve Eqs. (5.51) and (5.53) for pressure starting the calculation from surface to bottom varying grid index from L to 2.

iv. Check if steady state condition has been established in all the grid using: $\left|(Cs_i^{n+1} - Cs_i^n)/Cs_i^{n+1}\right| \leq \in \ \ (such\ as\ 1 \times 10^{-6})$.

v. If steady state has not reached, proceed to Step vi, else stop.

vi. Increment the time step; N = n+1. Go to Step 1 and repeat the procedures for other time steps.

CHAPTER 6: RESULTS AND DISCUSSIONS

In this chapter, model predictions for concentric horizontal annulus were compared with the experimental data presented by Chen (2005). After calibrating the model, sensitivity analysis was conducted considering the three-segment well profile presented in Section 4.3.1. The sensitivity analysis with respect to drilling parameters was performed to investigate hole cleaning performance of foam and present ways to optimize it. In addition, parametric study was conducted to examine the effect of water-influx during foam drilling in vertical wells.

6.1 Comparison of Model Predictions with Experimental Measurements

Chen (2005) carried out cuttings transport experiments with foam at ambient temperature (80°F) and low pressure conditions (100 psi) in a concentric horizontal annulus. The effects of foam quality, polymer concentration and flow velocity on cuttings transport in horizontal annulus were experimentally investigated. Tests were conducted at different foam qualities varying from 0.7 to 0.9. At each foam quality, polymer concentration and foam velocity were varied from 0 to 0.5% and 2 to 6 ft/s, respectively. Other test parameters are presented in Table 6.1.

Table 6.1 Test parameters for cuttings transport experiments (Chen 2005)

Parameters	Value	Unit
Liquid density	8.3	ppg
Solid density	19	ppg
Drillpipe OD	3.5	inch
Inclination	90	Degrees
Hole size	5.76	inch
Particle size	0.12	inch
Back pressure	100	psi
Surface temperature	80	◦F

Test parameters presented in Table 6.1 are used to predict equilibrium cuttings concentration in the concentric horizontal annulus using the model. Subsequently, the model predictions are compared with the experimental data of Chen (2005). Figures 6.1 through 6.5 compare cuttings concentration prediction of the model with the experimental measurements obtained at 100 psi and 80°F for varying concentration of polymer (C_p). As the flow velocity increases, both measured and predicted cuttings concentration decreases. Also, with the increase in the foam quality, cuttings concentration obtained from both the experimental observation and model prediction decreases. This is attributed to the increase in viscous forces, which improves hole cleaning performance of the fluid.

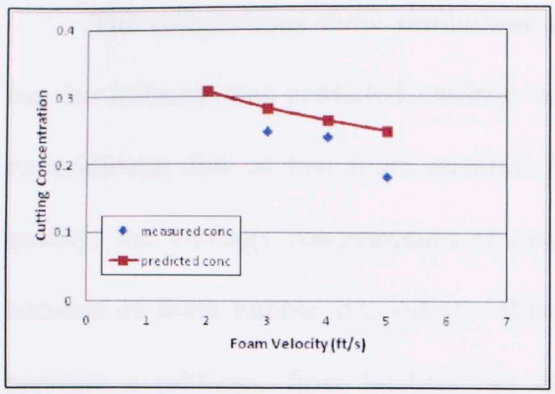

Fig. 6.1 Cuttings volumetric concentration vs. velocity (Γ=90% & CP =0%)

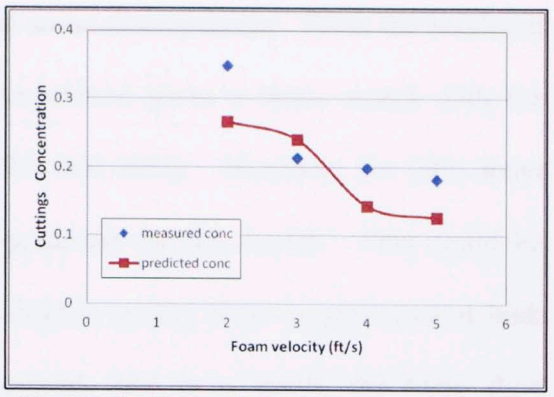

Fig. 6.2 Cuttings volumetric concentration vs. velocity (Γ=90% & CP =0.25%)

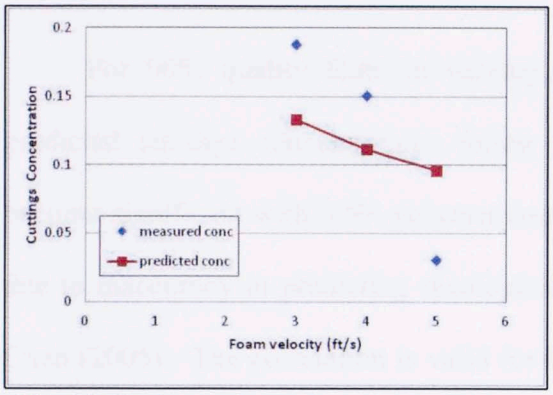

Fig. 6.3 Cuttings volumetric concentration vs. velocity (Γ=90% & CP =0.5%)

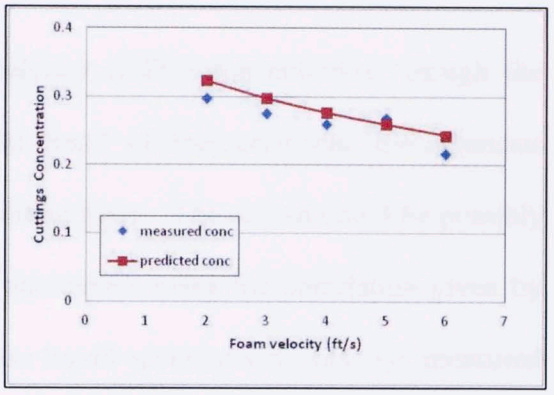

Fig. 6.4 Cuttings volumetric concentration vs. velocity (Γ=80%, CP =0%)

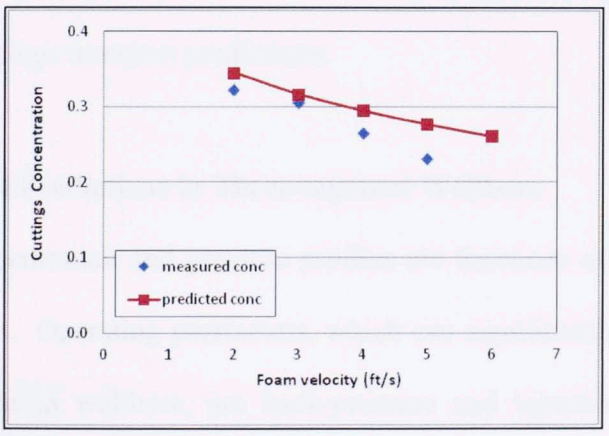

Fig. 6.5 Cuttings volumetric concentration vs. velocity (Γ=70%, C_P =0%)

The comparisons show similarities and some discrepancies. From the results, it can be inferred that predicted cuttings concentration gives a better match with the experimental data at low foam qualities (70% and 80%). However, for 90% foam quality, the cuttings concentration is over-predicted by the model. This could be because of foam bubble size effect. When higher quality foam is generated at high pressure conditions, finer bubbles are generated, and as a result, the foam flow properties deviate from the normal trend, affecting hole cleaning performance.

For 90% quality foam at varying polymer (HEC) concentration, though the predicted cuttings concentrations follow the trend of measurements, discrepancies become significant with 0.5% polymer containing foam. The reason could be possibly due to inaccuracy in predicting rheological parameters using the correlation given by Chen (2005). The correlation is valid for base liquid apparent viscosity (i.e. measured at 300 s^{-1}) ranging from 1 to 8.1 cp. However, the apparent viscosity of 0.5% HEC concentration is measured to be 8.1 cp, which is on the boundary line. Inaccurate prediction of rheological parameters such as consistency index can result in higher discrepancies in cuttings transport predictions.

6.2 Dynamic Model Predictions in Three-segment Wellbore

Cuttings concentration and pressure profiles are functions of drilling parameters and foam hydraulics. Operating parameters, which can significantly affect the cuttings concentration profile in wellbore, are back-pressure and injection rates of gas and liquid. For investigating hole-cleaning and pressure profile in eccentric annulus, a three-segment wellbore is considered as shown in Fig. 4.1. To perform a parametric

study, a well with 10,000 ft measured depth is considered. Numerical computations were performed using 50-ft long wellbore segments (computational grids). Lengths of wellbore sections are presented in Table 4.1. Sensitivity analysis was carried out by varying two important parameters: i) gas-injection rate; and ii) back-pressure. Drillpipe eccentricity of 50% is assumed with respect to hole. Liquid injection of 2 bbl/min was maintained constant for all cases. Other simulation parameters are presented in Table 6.2.

Table 6.2 Input data for foam cuttings transport simulation

Parameters	Values	Unit
Liquid density	8.3	ppg
Solid density	19	ppg
Liquid injection rate	2	bbl/min
Drillpipe OD	5	inch
Hole size	9	inch
Measured Depth	10000	ft
Dog-leg angle	3◦	per 100 ft
Particle size	0.15	inch
Rate of Penetration	150	ft/hr
Surface temperature	100	◦F
Temperature Gradient	1.2	◦F/100ft

6.2.1 Effect of Inclination on Cuttings Transport:

Cuttings concentration and pressure profiles change significantly with inclination during foam drilling. In conventional drilling, predicting the pressure profile is

straightforward; however, in foam drilling, difficulty lies in predicting the cuttings concentration and pressure profiles because of significant foam properties variation in the wellbore.

To investigate the effect of inclination on foam velocity and hole-cleaning, simulations were run for a three-segment wellbore. Back-pressure and gas-injection rate were maintained constant at 500 psi and 20 scf/s, respectively. Figures 6.6 and 6.7 show the variation of critical foam velocity and bed-height with inclination for steady state condition in the build-up section. At equilibrium condition, net torque acting on a particle is zero. Hence, using Eq. (5.41) the local velocity required to initiate particle movement (critical velocity) can be expressed as:

$$u^2 \approx \frac{4dg(s-1)\sin(\varphi+\alpha)}{3(C_D \sin\varphi + C_L \cos\varphi)} \tag{6.1}$$

As we can see from Fig. 6.6, local velocity near the bed increases with inclination until the inclination angle reaches 90-ϕ, where ϕ is the angle of repose. The critical velocity decreases thereafter, until the well becomes completely horizontal. Equation 6.1 clearly shows that the critical local foam velocity varies as a square root of the sine function. It has its maximum value at 90-ϕ. Theoretically, this indicate that wellbores with inclination angle of 90-ϕ are the most difficult to clean.

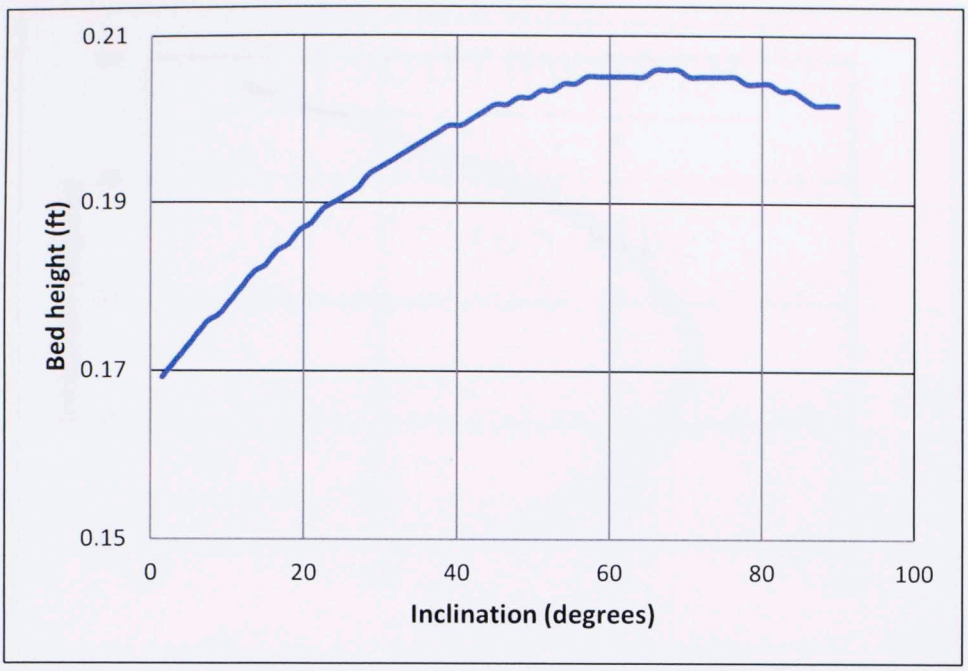

Fig. 6.7 Bed height vs. inclination angle

6.2.2 Effect of Gas-injection

Back pressure and liquid-injection rate were maintained constant at 500 psi and 2 bbl/min, respectively while the gas-injection rate was varied from 20 to 25 scf/s. Figures 6.8 through 6.10 show bed height, transient cuttings concentrations and pressure profiles along the three-segment wellbore.

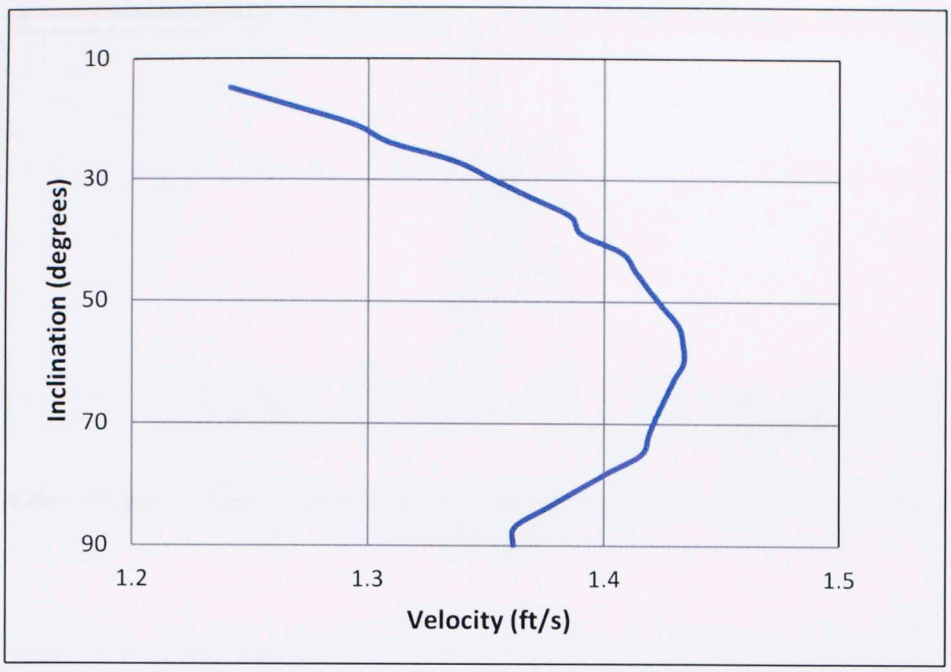

Fig. 6.6 Critical local velocity vs. inclination angle

For inclination angle between 0 and 90-ϕ, increased well inclination requires higher local fluid velocity to clean the wellbore. Thus, increasing the inclination angle at constant fluid flow rate, results in deposition of cuttings in the wellbore, which increases bed height and reduces flow area. The reduction in flow area increases the fluid velocity and prevents further deposition of cuttings. The process leads to a new steady state condition with increased inclination angle and equilibrium bed height as shown in Fig. 6.7. However, for inclination angle after 90-ϕ until the well becomes horizontal, fluid velocity required to clean the wellbore decreases. Consequently, bed-height at constant foam flow rate decreases thereafter as shown in Fig. 6.7; thus increasing the flow area and reducing the fluid velocity.

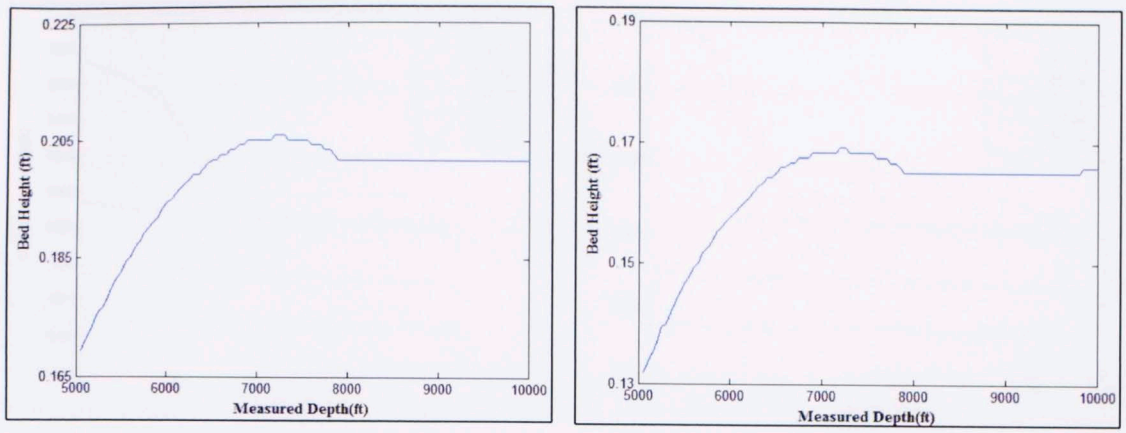

(a) (b)

Fig. 6.8 Bed height vs. depth in build-up and horizontal section: a) Q_g = 20 scf/s; and b) Q_g = 25 scf/s

Figure 6.8 shows the bed-height profile in the build-up and horizontal sections of the wellbore at different gas-injection rates. Under steady state condition, bed height increases with measured depth until it reaches its peak value at inclination angle of 90-ϕ. The formation of thick bed in this section creates a condition for stuck-pipe to occur. For inclination angles greater than 90-ϕ, bed height slightly decreases with the increase in inclination. This is due to the change in fluid velocity required for hole-cleaning. From Fig. 6.8, it can be observed that increased gas-injection rate reduced the bed-height from 0.21 to 0.17 ft. The bed height reduction is due to increase in foam viscosity resulting from higher gas injection rate, which increases foam quality and improves drag force acting on cuttings particles.

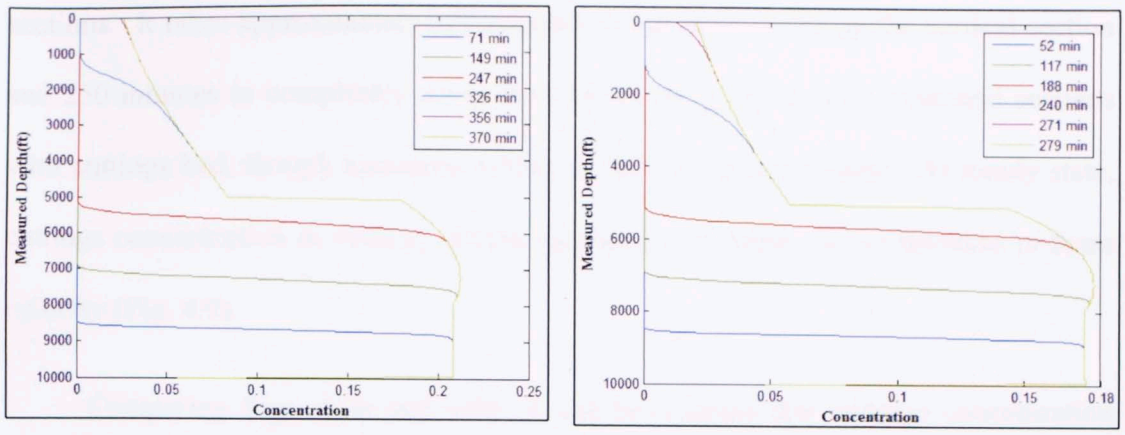

(a) (b)

Fig. 6.9 Transient cuttings volumetric concentration in three-segment well: a) Q_g = 20 scf/s; and b) Q_g = 25 scf/s

Figure 6.9 shows the cuttings concentration (including bed-height) as a function of time in the three-segment wellbore for different gas-injection rates. In the horizontal and build-up sections, cuttings accumulate on the low-side of the wellbore and move by rolling and bouncing along the wellbore. It can be observed from Fig. 6.9a that after 71 minutes of drilling, the bottom part of the wellbore is filled with cuttings. The bed front has reached 8500 ft of measured depth. Similarly, after 247 minutes, bed front has reached to bottom of the vertical section (5000 ft of measured depth). However, in the vertical section, cuttings no longer deposit in the wellbore and remain suspended in the fluid and move upward along the foam with slippage. As a result, cuttings concentration sharply decreases from 0.2 to 0.075 at 5000 ft of measured depth. After 326 minutes, although bed height in horizontal and build-up sections has reached the steady state condition, cuttings front still moving in the vertical section approaching 1000 ft depth. It is important to note that cuttings front moves faster in vertical section than the build-up and horizontal sections. This is due to complete suspension of cuttings in fluid as compared to deposition of cuttings in the build-up and horizontal

sections. It takes approximately 120 minutes for cuttings to fill-up the vertical section and 250 minutes to completely cover low-side of the build-up and horizontal sections with cuttings bed, though measured depths of both sections are same. At steady state, cuttings concentration in vertical section increases with depth due to decrease in foam velocity (Fig. 4.9).

Comparing Figs. 6.9a and 6.9b, it can be inferred that cuttings concentration increases in the three-segment well as the gas-injection rate is reduced. Bottom-hole and surface cuttings concentration are 0.22 and 0.04, respectively for 20 scf/s gas-injection rate while increasing the injection rate to 25 scf/s reduces the bottom-hole and surface cuttings concentration to 0.17 and 0.025, respectively. Furthermore, at lower flow rate (20 scf/s), it takes more time (370 minutes) for the cuttings to reach the steady state condition because of the decrease in foam velocity, which reduces cutting front velocity.

Figure 6.10 shows the transient pressure profile as a function of measured depth. Initially, pressure at the bottom of hole increases slowly with time as the cuttings bed form in the horizontal and highly inclined (build-up) sections. This is because of the increase in friction pressure loss. As the cuttings reach the vertical section, additional hydrostatic pressure gradient due to cuttings causes further compression of foam and higher pressure drop with depth. It can be observed from Fig. 6.10a that until 247 minutes, increase in bottom-hole pressure is gradual (100 psi). Then, the bottom-hole pressure increases more rapidly (i.e. 200 psi in 120 minutes). Comparing Figs. 6.10a and 6.10b, pressure along the wellbore increases as the gas-injection rate is reduced due to reduction in gas fraction and hence increase in foam density. Bottom-hole pressure is

2100 psi at 20 scf/s while it decreases to 1900 psi at increases gas-injection rate of 25 scf/s.

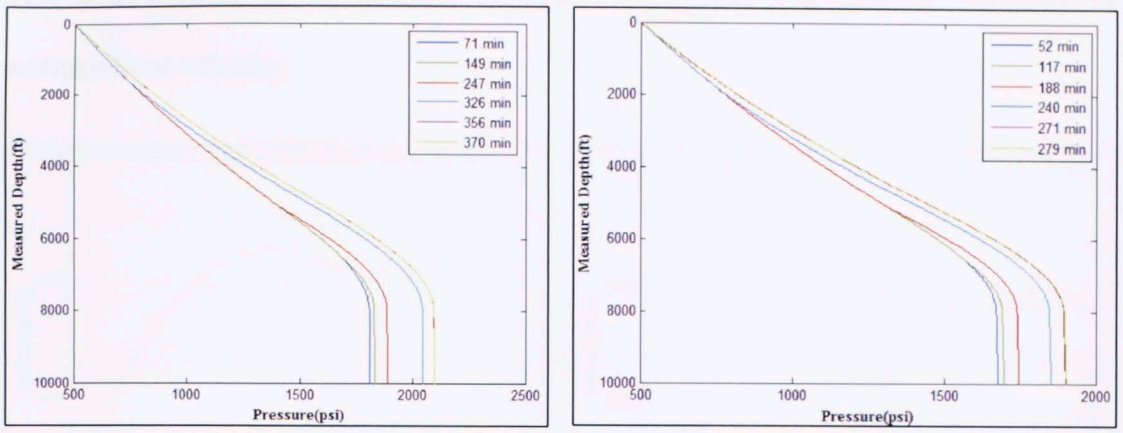

(a) (b)

Fig. 6.10 Transient pressure profile in three-segment well: a) Q_g = 20 scf/s; and b) Q_g = 25 scf/s

6.2.3 Effect of Back Pressure

Simulations were run for different back-pressures of 300 psi and 500 psi while liquid-injection rate and gas-injection rate were maintained constant at 2 bbl/min and 20 scf/s, respectively. The effect of back pressure on bed height in the build-up and horizontal sections is shown in Fig. 6.11. Bed-height increases as the back-pressure is increased. This is because of the decrease in foam quality, velocity (Fig. 4.3) and viscosity (Fig. 4.5) with increase in back-pressure resulting in poor hole cleaning and increased bed-height. From Fig. 6.12, it can be inferred that cuttings concentration is relatively higher at higher back-pressure of 500 psi. Bottom-hole and surface cuttings concentration are 0.22 and 0.04, respectively for 500 psi back-pressure while lowering the back-pressure to 300 psi reduces the bottom-hole and surface cuttings concentration

to 0.18 and 0.02, respectively. Furthermore, it takes more time (370 minutes) to establish steady state condition at 500 psi back-pressure than 300 psi back-pressure. This is as a result of the decrease in foam velocity and consequently, reduction in cuttings front velocity.

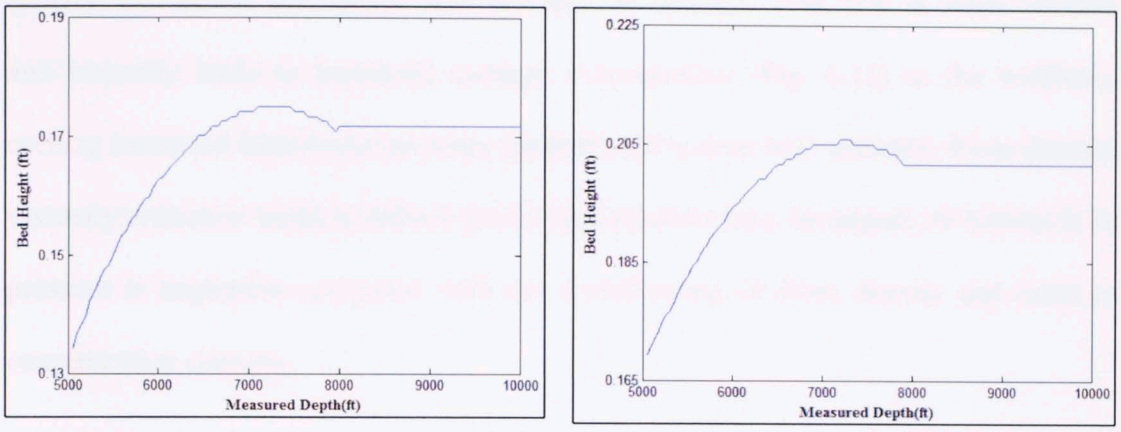

(a) (b)

Fig. 6.11 Bed-height in build-up and horizontal section: a) P_b = 300 psi; and b) P_b = 500 psi

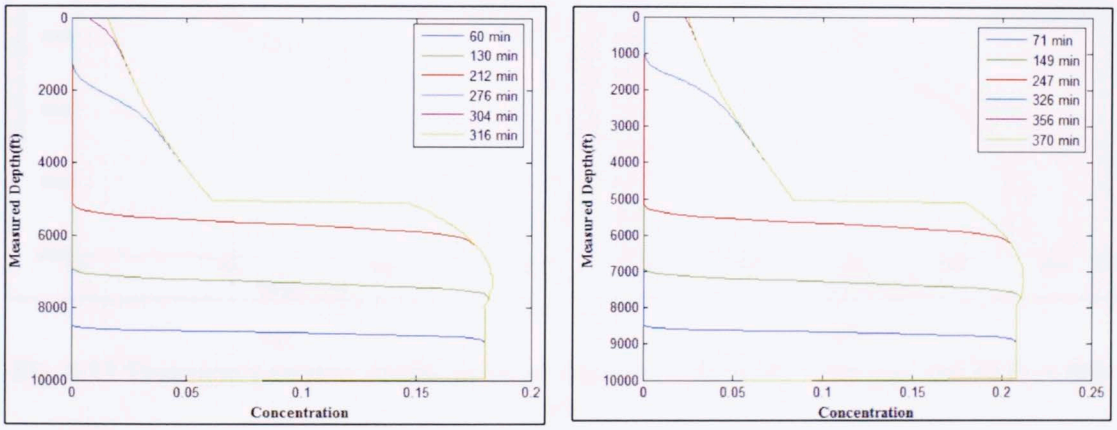

(a) (b)

Fig. 6.12 Transient cuttings volumetric concentration profile in three-segment well: a) P_b =300 psi; and b) P_b = 500 psi

Back-pressure has significant impact on the bottom hole pressure during underbalanced drilling. As the simulation results show in Fig. 6.13, bottom hole pressure has increased from 1600 psi to 2100 psi when the back-pressure is increased

from 300 to 500 psi. In foam drilling, back-pressure has primary and secondary effects on bottom hole pressure. The 200 psi in bottom-hole pressure increase is due to the primary effect. The remaining 300 psi increase is as a result of secondary effects such as contraction of foam or reduction of foam quality in the wellbore, which increases foam density; and hence, the bottom hole pressure. In addition, reduction in foam velocity and viscosity leads to increased cuttings concentration (Fig. 6.12) in the wellbore, causing increased hydrostatic pressure gradient and bottom hole pressure. Even though, viscosity reduction tends to reduce the friction pressure loss, its impact on bottom hole pressure is negligible compared with the contributions of foam density and cuttings concentration changes.

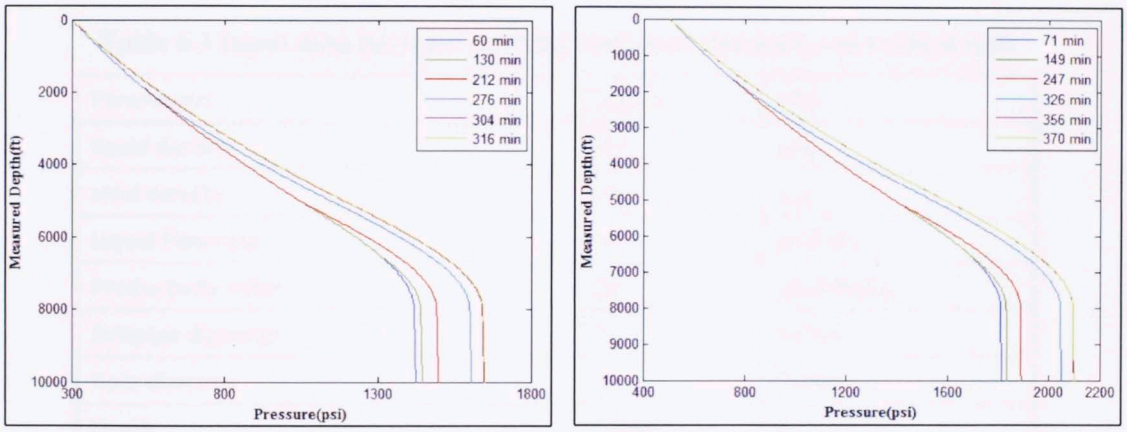

(a) (b)

Fig. 6.13 Transient pressure profile in three-segment well: a) P_b = 300 psi; and b) P_b = 500 psi

6.3 Dynamic Model Predictions with Water-Influx in Vertical Wellbore

Influx of liquid or gas during foam drilling is not quite uncommon. Liquid influx due to underbalanced conditions reduces the quality of foam and makes the foam less viscous causing hole cleaning problems. Though proactive measures can be taken to

avoid excessive influx, uncertainty of pore pressure and complexity of underbalanced drilling can result in large quantity of water influx. To investigate the effect of water-influx on foam properties and pressure profile, a parametric study was performed assuming vertical well of depth 10,000 ft. Simulation input parameters are given in Table 6.3. After running the foam-cuttings transport simulation keeping other drilling parameters (back-pressure, liquid and gas-injection rate) constant, bottom-hole pressure was found to be 1940 psi. A pore-pressure of 2110 psi is assumed for a reservoir having a productivity index of 20 bbl/day/psi to create a drawdown, which results in a water influx given by:

$$\text{Water influx rate} = (Productivity\ index \times drawdown) = 23.36 \text{ gal/min}$$

Table 6.3 Input data for foam cuttings transport simulation in vertical well

Parameters	Values	Unit
liquid density	8.3	ppg
solid density	19	ppg
Liquid Flow rate	2	bbl/min
Productivity Index	20	bbl/day/psi
Drillpipe diameter	5	inches
Hole diameter	9	inches
Depth	10000	ft
Pore pressure	2110	psi
Particle size	0.15	in
Rate of Penetration	150	ft/hr
Surface temperature	100	◦F
Temperature Gradient	1.2	◦F/100ft
Foam quality at surface	90%	
Back-pressure	300	psi

Finally, the water-influx rate is included in the material balance model to predict the changes in foam properties, and subsequently hole-cleaning. Figures 6.14 through 6.18 show the foam quality, foam velocity, transient cuttings concentration, pressure and ECD profiles along the depth. With water-influx, there is a reduction in foam quality along the wellbore. This happens because water influx increases the fraction of water in foam. In addition, the increase in foam density results in increased pressure in the wellbore, which compresses the foam leading to further reduction in bottom-hole quality. Consequently, bottom-hole quality reduces significantly from 0.65 to 0.5 because of the water-influx while surface quality decreases from 0.9 to 0.85 (Fig. 6.14).

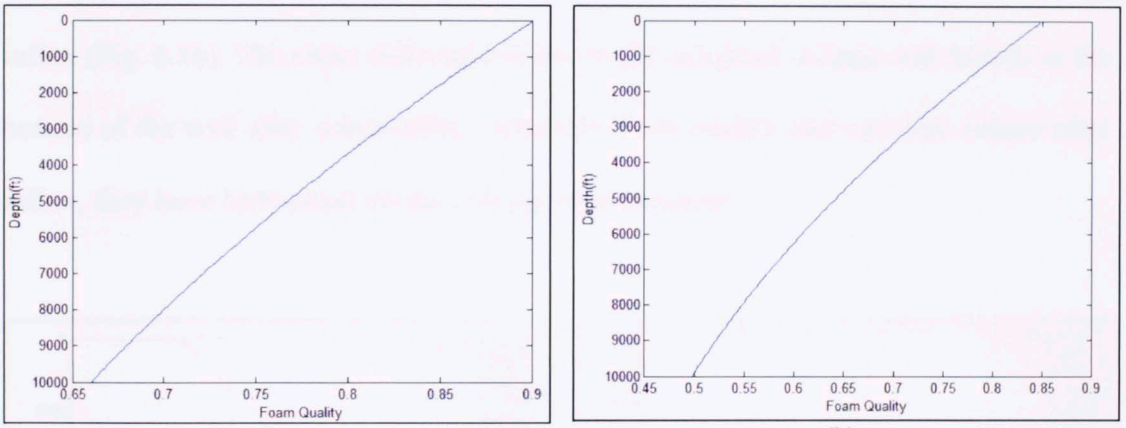

(a) (b)

Fig. 6.14 Foam quality profile: a) without water-influx; and b) with water-influx

In spite of substantial amount of water-influx rate, increase in foam velocity is minimal (Fig 6.15). This happens because additional hydrostatic pressure gradient due to water influx causes contraction of the foam and offsets any additional increase in volume. Only minor increase (6.1 to 6.5 ft/s) in surface foam velocity is observed with water-influx.

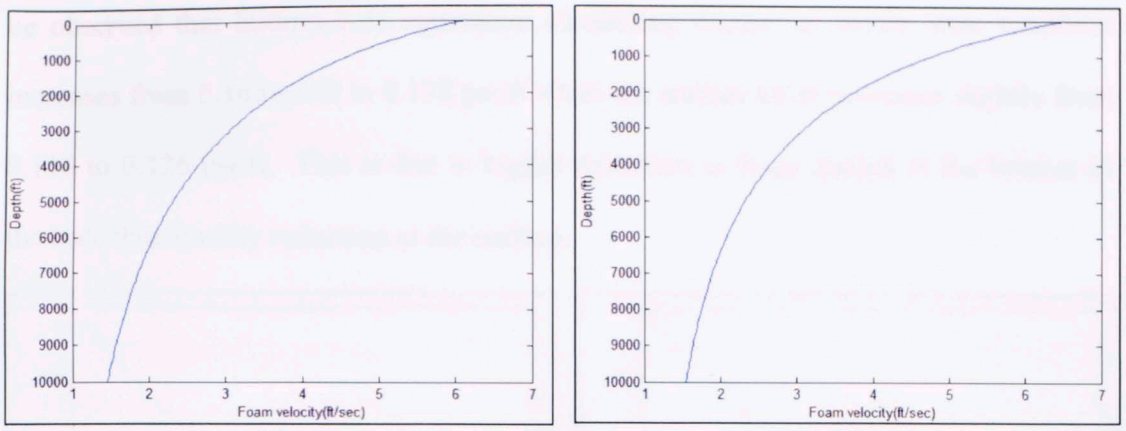

(a) (b)

Fig. 6.15 Foam velocity profile: a) without water-influx; and b) with water-influx

Equilibrium cuttings concentration profile remains almost the same. Bottom-hole cuttings concentration slightly decreases from 0.039 to 0.037 because of water-influx (Fig. 6.16). The slight difference is due to the increased volume and density at the bottom of the well after water-influx. Although foam quality and viscosity reduce after influx, they have little effect on the cuttings concentration.

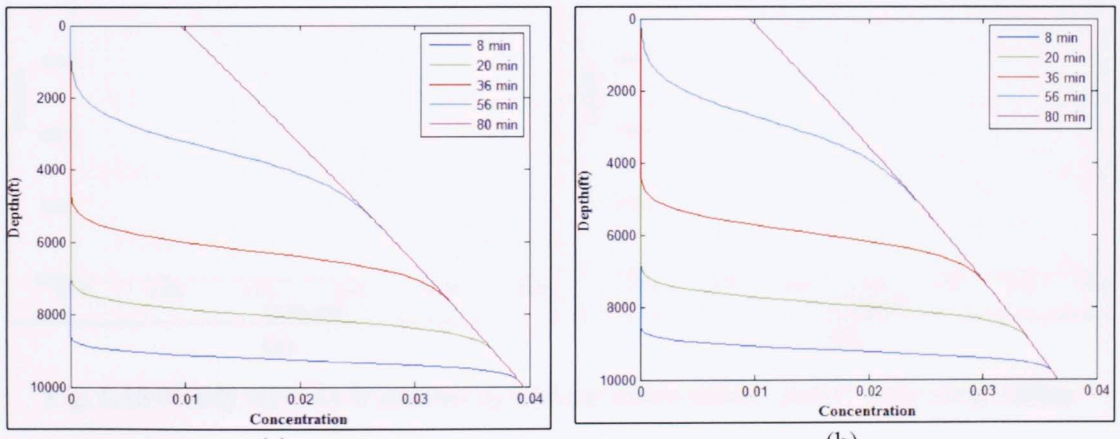

(a) (b)

Fig. 6.16 Transient cuttings volumetric concentration: a) without water-influx; and b) with water-influx

Bottom-hole pressure at steady state condition is 1950 psi without water-influx. However, with water-influx, it increases to 2100 psi (Fig. 6.17). From Fig. 6.18, it can

be observed that bottom-hole equivalent circulating density at steady state condition increases from 0.165 psi/ft to 0.178 psi/ft while the surface ECD increases slightly from 0.118 to 0.126 psi/ft. This is due to higher reduction in foam quality at the bottom of the hole than quality reduction at the surface.

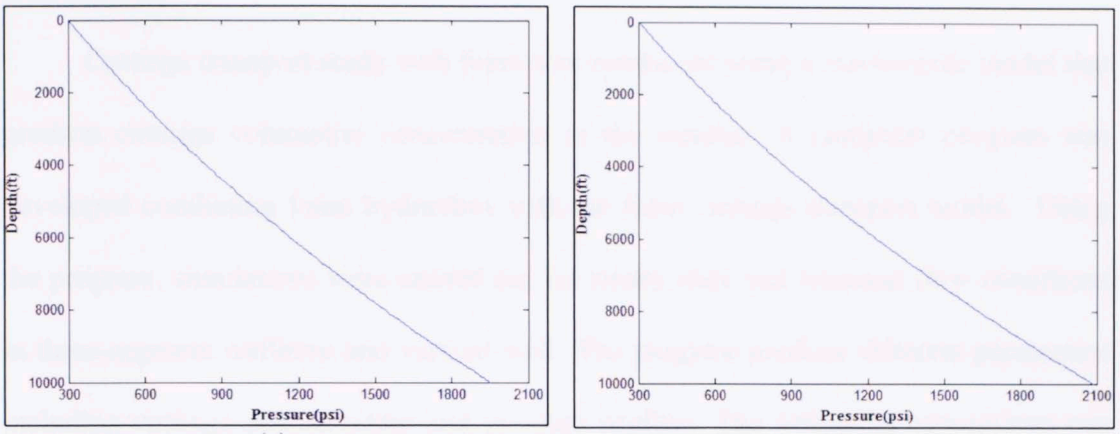

(a) (b)

Fig. 6.17 Steady state pressure profile: a) without water-influx; and b) with water-influx

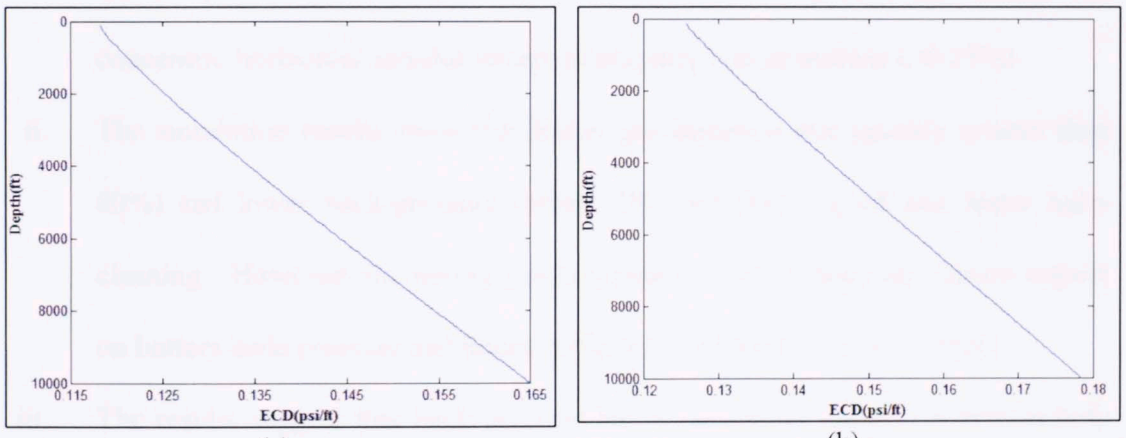

(a) (b)

Fig. 6.18 Steady state ECD profile: a) without water-influx; and b) with water-influx

CHAPTER 7: CONCLUSIONS AND RECOMMENDATIONS

Conclusions

Cuttings transport study with foam was conducted using a mechanistic model that predicts cuttings volumetric concentration in the annulus. A computer program was developed combining foam hydraulics with the foam cuttings transport model. Using the program, simulations were carried out for steady state and transient flow conditions in three-segment wellbore and vertical well. The program predicts different parameters including cuttings concentration and pressure profiles. The following conclusions can be deduced from the study.

i. Model predictions showed a good match with experimental results for concentric horizontal annulus except at polymer concentrations (>0.25%).

ii. The simulation results show that higher gas-injection rate (quality greater than 80%) and lower back-pressure (below 500 psi) favors good and faster hole-cleaning. However, increasing gas-injection rate can reduce any abrupt impact on bottom-hole pressure and hence preferred over back-pressure control.

iii. The results suggest that back-pressure has a significant impact on bottom-hole pressure without affecting much of its hole-cleaning capacity and can be used for instant adjustment in bottom-hole pressure. However, gas-injection rate has a gradual impact on changing the bottom-hole pressure.

iv. Gas and liquid-injection rates, back-pressure and inclination impact the time taken for the cuttings to reach to the surface and stabilize the bottom-hole

pressure. Cuttings move much faster in vertical section as compared to the deviated sections.

v. Foam has a tendency to absorb plenty of formation water during water-influx causing reduction in quality by as much as 23 %. However, reduction in its hole-cleaning capacity is minimal and determined by the amount of influx rate.

vi. Hole-cleaning is a function of inclination. The result shows that bed height increases with increasing inclination angle until it reaches 90-ϕ and then reduces creating suitable condition for stuck-pipe to occur.

Recommendations

i. Addition of appropriate polymer concentration to the base liquid is recommended to give viscosity and stability to the foam.

ii. Foam is preferable in drilling horizontal wells with long displacement. Foam properties remain more consistent and intact in horizontal section. This helps in the stability of foam and mitigating any undesirable variation in bed-height and pressure profile.

iii. It is recommended to predict real-time cuttings concentration and pressure profile to proactively forecast the impact of changing drilling parameters.

iv. In case of water-influx, it is recommended to keep observing the foam quality at the annulus. Reduction in the foam quality during influx can be maintained by increasing the gas injection rate and adjusting the back pressure simultaneously to maintain the desired underbalance.

Recommendation for Further Study

i. Since the particles may vary both in size and shape, it is necessary to study the effect of different particle sizes and shapes on the cuttings concentration and the pressure profiles along the wellbore.

ii. Pipe rotation has a major effect on the cuttings concentration distribution in the annulus. Hence, it is necessary to study the effect of pipe rotation on cuttings concentration in the annulus.

iii. Study of the effect of wide range of foam-quality, different polymer concentration and stability period of foam is necessary to design foam before underbalanced drilling.

iv. Further study on improving the local stress and local velocity in the eccentric annulus is necessary to accurately predict the equilibrium bed height in the horizontal section of a wellbore.

REFERENCES

Ahmed, R., Kuru, E. and Arild, S. 2003a. Critical Review of Drilling Foam Rheology. *Annual Transactions of the Nordic Rheology Society,* 11, 2003.

Ahmed, R., Kuru, E. and Arild, S. 2003b. Mathematical Modeling of Drilling Foam Flows. Paper 2003-003 presented at the CADE/CAODC Drilling Conference, Calgary, Alberta, Canada, October 20-22, 2003.

Ahmed, R., Skalle, P. and Johansen, S. 2003c. A Mechanistic Model to Determine the Critical Flow Velocity Required to Initiate the Movement of Spherical Bed Particles in Inclined Channels. Chemical Engineering Science 58 (2003): 2153-2163.

Ahmed, R. and Miska, S. Z. 2009. *Advanced Drilling and Well Technology,* 191-221. Richardson, Texas, SPE.

Aworunse, O.A. 2012. Modeling of Power-Law Fluid Flow in Annulus with Cuttings Bed Buildup. MS Thesis, University of Oklahoma, Norman, Oklahoma

Beyer, A.H., Millhone, R.S. and Foote, R.W. 1972. Flow Behavior of Foam as a Well Circulating Fluid. Paper SPE 3986 presented at the 47th Annual Fall Meeting, San Antonio-Texas, October 8-11, 1972.

Blauer, R.E., Mitchell, B.J. and Kohlhaas, C.A. 1974. Determination of Laminar, Turbulent and Transitional Foam Flow Losses in Pipes. Paper SPE 4885 presented at the SPE 44th Annual California Regional Meeting, San Francisco-California, April 4-5, 1974.

Capo, J. 2002. Cuttings Transport with Foam at Intermediate Inclination Angles. M.S. Thesis, The University of Tulsa, Tulsa, Oklahoma 2002.

Carmichael, K.E. 1995. On the Outlet Boundary Condition for Solids Leaving Slurry-bubble Columns. *The Chemical Engineering Journal* 57: 299-301.

Chen, Zhu. 2005. Cuttings Transport with Foam in Horizontal Concentric Annulus under Elevated Pressure and Temperature Conditions. Ph.D. Dissertation, The University of Tulsa, Tulsa, Oklahoma 2005.

Chen, Z., Ahmed, R., Miska,S., Takach, N., Yu, M. and Pickell, M. 2005. Rheology and Hydraulics of Polymer (HEC)-Based Drilling Foams at Ambient Temperature Conditions. Paper SPE 94273 presented at the 2005 SPE Production and Operations Symposium, Oklahoma City, Oklahoma, 17-19 April.

Cho, H., Shah, S.N., Osisanya, S.O. 2000. A Three-Segment Hydraulic Model for Cuttings Transport in Horizontal and Deviated Wells. Paper SPE 65488 presented at the SPE/Petroleum Society of CIM International Conference on Horizontal Well Technology, Calgary, Alberta, Canada 6-8 November, 2000.

Civan, F. 1996. A Multi-purpose Formation Damage Model. Paper SPE 31101 presented at the SPE Formation Damage Control Symposium, Lafayette, Louisiana 14-15 February, 1996.

Civan, F. 2007. *Reservoir Formation Damage Fundamentals, Modeling, Assessment and Mitigation.* 2nd ed., Gulf Professional Publishing, 2007: 1016-1017.

Duan, M. 2005. An Experimental Study of Small Sand-Sized Cuttings Transport in Horizontal and High Angle Boreholes. MS Dissertation, University of Tulsa, Tulsa, OK.

Duan, M., Miska, S., Yu, M. and Takach, N. 2008. Experimental Study and Modeling of Cuttings Transport using Foam with Drill-pipe Rotation. Paper SPE 116300 presented at the SPE Annual Technical Conference and Exhibition, Denver, 21-24 September 2008.

Eisenthal, R. and Cornish-Bowden, A. 1974. *BioChem. J.* 139: 715.

El-Samni, E.A. and Einstein, H.A. 1949. Hydrodynamic Forces on a Rough Wall. *Reviews of Modern Physics* 21(3): 520-524.

Fredrickson, A.G. and Bird, R.B. 1958. Non-Newtonian Flow in Annuli. *Industrial and Engineering Chemistry Research* 50; 347-383.

Gardiner, B.S., Dlugogorski, B.Z. and Jameson, G.J. 1998. Rheology of Fire-Fighting Foams. *Fire Safety Journal*, 1998.

Hatschek, E. 1911. Die Viskositat der Dispersoide. *Kolloid-Z*: 34-39.

Ibizugbe, N.O. 2012. Drainage Behavior of Oil-Based Drilling Foam under Ambient Conditions. MS Thesis, University of Oklahoma, Norman-OK.

Ityokumbul, M.R. 1994. A Non-Parametric Method for Particle Settling Velocity Determination in a Slurry Bubble Column. *The Chemical Engineering Journal* 54: 1-6.

Iyoho, A.W., Horeth II, J.M., and Veenkant, R.L. 1988. A Computer Model for Hole-Cleaning Analysis. *Journal of Petroleum Technology*, September 1988 40(9): 1183-1192.

Koehler, S.A., Hilgenfeldt, S. and Stone, H.A. 1999. Liquid Flow through Aqueous Foams: The Node-Dominated Foam Drainage Equation. *Phys. Rev. Lett.* 82, 4232.

Kuru, E. and Osunde, O. 2006. Numerical Modeling of Cuttings Transport with Foam in Inclined Wells. PETSOC Paper 2006-071 presented at the Petroleum Society's 7th Canadian International Petroleum Conference, Calgary, Alberta, Canada, June 13-15, 2006.

Laird, W. 1957. Slurry and Suspension Transport-Basic Flow Studies on Bingham Plastic Fluids. *Ind. Eng.Chem.*, 49(1); 138-141.

Li, Y. 2004. Numerical Modeling of Cuttings Transport with Foam in Vertical and Horizontal Wells. Ph.D. Dissertation, University of Alberta, Calgary, Canada 2004.

Lourenco, A.M.F. 2002. Study of Foam flow under Simulated Down-hole Conditions. MS Thesis, University of Tulsa, Tulsa, Oklahoma.

Luo, Y., Peden, J.M. 1987. Flow of Non-Newtonian Fluids through Eccentric Annuli. Paper SPE 16692 presented at the SPE Annual Technical Conference and Exhibition. Dallas, September 27-30.

Martins, A.L., Santana, M.L., Campos, M. and Gaspar, E.F. 1998. Evaluating the Transport of Solids Generated by Shale Instabilities in ERW Drilling. Paper SPE 50380 presented at the SPE International Conference on Horizontal Well Technology. Calgary, Alberta, 1-4 November, 1998.

Melrose, J.C., Savins, J.G., Foster, W.R. and Parish, E.R. 1958. A practical Utilization of the Theory of Bingham Plastic Flow in Stationary Pipes and Annuli. *Petroleum Transaction, AIME*, 213, 1958.

Mitchell, B.J. 1969. Viscosity of Foam. PhD Dissertation, University of Oklahoma, Norman, Oklahoma.

Okpobiri, G.A, and Ikoku, C.U. 1983. Experimental Determination of Friction Factors for Mist and Foam Drilling and Well Cleanout Operations. *Journal of Energy Resources Technology* 105(1983): 542-553.

Owayed, J.F. 1997. Simulation of Water Influx during underbalanced Foam drilling. MS Thesis, University of Tulsa, Tulsa, OK.

Ozbayoglu, M.E. 2002. Cuttings Transport with Foam in Horizontal and Highly Inclined Wellbores. Ph.D. Dissertation, The University of Tulsa, Tulsa, Oklahoma 2002.

Sanghani, V. 1982. Rheology of Foam and its Implications in Drilling and Clean-Out Operations. M.S Thesis, University of Tulsa, Tulsa, Oklahoma 1982.

Shah, S.N., Khade, S.D. 2004. New Rheological Correlations for Guar Foam Fluids. *SPE Production and Facilites*, May 2004 19(2): 77-85.

Valko, P., and Economides, M.J. 1992. Volume Equalized Constitutive Equations for Foamed polymer solutions. *Journal of Rheology*, 6: 1033-1055.

Vaughn, R.D. and Grace, W.R. 1965. Axial Laminar Flow of Non-Newtonian Fluids in Narrow Eccentric Annuli. *SPE Journal*, 5 (4): 277-280.

Von Phul, S.A. and Lon Stern. 2004. Antifoam: What is it? How does it work? Weatherford incorporated foam project, Texas.

White, F.M. 1991. *Viscous Fluid Flow*, 2nd ed., 181-200. New York: McGraw-Hill.

NOMENCLATURE

β	=	momentum correction factor
β_c	=	Slip coefficient
d_{hyd}	=	hydraulic diameter of annulus
K_{foam}	=	Foam consistency index
K_{liquid}	=	Base liquid consistency index
n	=	fluid behavior index
Γ	=	foam quality
μ_L	=	base liquid viscosity
μ_F	=	foam apparent viscosity
ρ_{liquid}	=	Liquid density
Z	=	gas compressibility factor
τ_w	=	wall shear stress
ρ_s	=	density of solid cuttings
ρ_f	=	density of foam
S_s	=	density ratio of cuttings to foam fluid
v_s	=	slip velocity between fluid and solid particles
v	=	mean foam velocity in annulus
ROP	=	rate of penetration
D_h	=	Diameter of hole
d	=	particle diameter

φ = Angle of repose

Re_p = Reynolds number of particle

a_v = vertical component of the distance between the wellbore center and the drillpipe center

h_{low} = vertical height from the wellbore bottom to the drillpipe bottom

h_{high} = vertical height from the wellbore bottom to the drillpipe top

e = eccentricity of pipe

S = total wetted parameter

S_o = wetted perimeter of the outer wellbore

S_i = wetted perimeter of the inner drillpipe wall

S_b = wetted perimeter of a cuttings bed

A_f = fluid flow area above the cuttings bed

$G(Z, n)$ = Geometry factor as a function of Z and n

T_{pr} = Pseudo-reduced temperature

P_{pr} = Pseudo-reduced pressure

D_o = Outer casing diameter

D_i = Inner pipe diameter

u = Local velocity at the center of particle

A = Projected area of cuttings

A_{ann} = Annular area

APPENDIX A

GENERAL CONFIGURATION OF ECCENTRIC ANNULUS GEOMETRY

Partially blocked annular geometry occurring in inclined and horizontal wellbores is shown in Fig. A.1. To determine the relative position of the pipe with respect to the wellbore, eccentricity is defined.

$$e = \frac{a}{R-r} \tag{A.1}$$

where, 'R-r' is the difference between the radii of the wellbore and the pipe, and 'a' is the offset distance between the centre of the wellbore and the centre of the pipe. Eccentricity is positive when the drillpipe centre is below the centre of the wellbore and negative when it is above the wellbore centre. Also, the eccentricity has direction and the pipe can align in the horizontal direction as in the vertical direction. However, in this study, the horizontal shift is not considered.

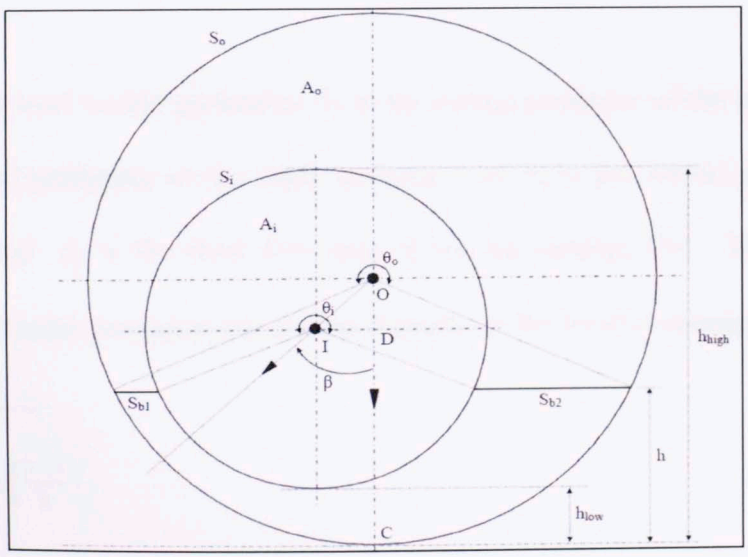

Fig. A.1 General Wellbore geometry configuration (Duan 2005)

Denoting a_v as the vertical component of the distance between the wellbore center and the drillpipe center, a_v can be expressed as:

$$a_v = (R - r)e \cos \beta \tag{A.2}$$

where, h_{low} is the vertical height from the wellbore bottom to the drillpipe bottom and h_{high} is the vertical height from the wellbore bottom to the drillpipe top. The vertical heights are expressed as:

$$h_{low} = R - r - a_v \tag{A.3}$$

$$h_{high} = R + r - a_v \tag{A.4}$$

For a given bed height, total wetted perimeter and area can be calculated as:

$$S = S_o + S_i + S_b \tag{A.5}$$

$$A_o = A_f + A_i \tag{A.6}$$

where, S is the total wetted parameter, S_o is the wetted perimeter of the outer wellbore, S_i is the wetted perimeter of the inner drillpipe wall, S_b is the wetted perimeter of a cuttings bed and A_f is the fluid flow area above the cuttings bed. The calculation procedure of annular geometric parameters depends on the level of cuttings bed height.

Case1: $h < h_{low}$

$\theta_0 = 2arccos\left(\frac{h-R}{R}\right)$

$\theta_i = 2\pi$

$$S_o = R\theta_o$$

$$S_i = r\theta_i$$

$$S_b = 2\sqrt{R^2 - (R-h)^2}$$

$$A_o = R^2 \frac{\theta_o}{2} + (R-h)\sqrt{R^2 - (R-h)^2}$$

$$A_i = r^2 \frac{\theta_i}{2}$$

Therefore,

$$S = 2Rarccos\left(\frac{h-R}{R}\right) + 2\pi r + 2\sqrt{R^2 - (R-h)^2}$$

$$A_f = R^2 arccos\left(\frac{h-R}{R}\right) + (R-h)\sqrt{R^2 - (R-h)^2} - \pi r^2$$

Case 2: $h_{low} < h < h_{high}$

$$S = 2Rarccos\left(\frac{h-R}{R}\right) + 2rarccos\left[\frac{h-R+a_v}{r}\right] + 2\sqrt{R^2 - (R-h)^2} - 2\sqrt{r^2 - [R-h-a_v]^2}$$

$$A_f = R^2 arccos\left(\frac{h-R}{R}\right) + (R-h)\sqrt{R^2 - (R-h)^2} - r^2 arccos\left(\frac{h-R+a_v}{r}\right) - [R-h-a_v]\sqrt{r^2 - [R-h-a_v]^2}$$

Case 3: $h > h_{high}$

$$S = 2Rarccos\left(\frac{h-R}{R}\right) + 2\sqrt{R^2 - (R-h)^2}$$

$$A_f = R^2 arccos\left(\frac{h-R}{R}\right) + (R-h)\sqrt{R^2 - (R-h)^2}$$